POLYPUBLIE
Polytechnique Montréal

POLYTECHNIQUE MONTRÉAL
UNIVERSITÉ D'INGÉNIERIE

Titre: Title:	Solid hold-up measurement in a jet-impactor assisted fluidized bed using gamma-ray densitometry
Auteurs: Authors:	Hamed Nasri Lari, Majid Rasouli, Jamal Chaouki, & Jason Robert Tavares
Date:	2020
Type:	Article de revue / Article
Référence: Citation:	Nasri Lari, H., Rasouli, M., Chaouki, J., & Tavares, J. R. (2020). Solid hold-up measurement in a jet-impactor assisted fluidized bed using gamma-ray densitometry. AIChE Journal, 66(11), e16653 (14 pages). https://doi.org/10.1002/aic.16653

Document en libre accès dans PolyPublie
Open Access document in PolyPublie

URL de PolyPublie: PolyPublie URL:	https://publications.polymtl.ca/10445/
Version:	Version finale avant publication / Accepted version Révisé par les pairs / Refereed
Conditions d'utilisation: Terms of Use:	Tous droits réservés / All rights reserved

Document publié chez l'éditeur officiel
Document issued by the official publisher

Titre de la revue: Journal Title:	AIChE Journal (vol. 66, no. 11)
Maison d'édition: Publisher:	Wiley
URL officiel: Official URL:	https://doi.org/10.1002/aic.16653
Mention légale: Legal notice:	This is the peer reviewed version of the following article: Nasri Lari, H., Rasouli, M., Chaouki, J., & Tavares, J. R. (2020). Solid hold-up measurement in a jet-impactor assisted fluidized bed using gamma-ray densitometry. AIChE Journal, 66(11), e16653 (14 pages). https://doi.org/10.1002/aic.16653, which has been published in final form at https://doi.org/10.1002/aic.16653. This article may be used for non-commercial purposes in accordance with Wiley Terms and Conditions for Use of Self-Archived Versions. This article may not be enhanced, enriched or otherwise transformed into a derivative work, without express permission from Wiley or by statutory rights under applicable legislation. Copyright notices must not be removed, obscured or modified. The article must be linked to Wiley's version of record on Wiley Online Library and any embedding, framing or otherwise making available the article or pages thereof by third parties from platforms, services and websites other than Wiley Online Library must be prohibited.

Solid Hold-Up Measurement in a Jet-Impactor Assisted Fluidized Bed Using Gamma-ray Densitometry

Journal:	*AIChE Journal*
Manuscript ID	AIChE-19-22318.R2
Wiley - Manuscript type:	Research Article
Date Submitted by the Author:	n/a
Complete List of Authors:	Nasri Lari, Hamed; Polytechnique Montreal, Chemical Engineering Rasouli, Majid; Ecole Polytechnique de Montréal, Chemical Engineering Chaouki, Jamal; +ëcole Polytechnique de Montr+¬al, D+¬partement de g+¬nie chimique Tavares, Jason Robert; Polytechnique Montreal, ;
Keywords:	Fluidization, Nanotechnology, Computational fluid dynamics (CFD), Particle/count/measurements, Particulate flows

SCHOLARONE™
Manuscripts

1
2
3
4
5
6
7
8
9
10
11
12
13
14
15
16
17
18
19
20
21
22
23
24
25
26
27
28
29
30
31
32
33
34
35
36
37
38
39
40
41
42
43
44
45
46
47
48
49
50
51
52
53
54
55
56
57
58
59
60

Solid Hold-Up Measurement in a Jet-Impactor Assisted Fluidized Bed Using Gamma-ray Densitometry

Hamed Nasri Lari, Majid Rasouli, Jamal Chaouki, Jason R. Tavares[*]

---

[*] Corresponding author: jason.tavares@polymtl.ca

Department of Chemical Engineering, Polytechnique Montreal, Montreal, QC, Canada H3C 3A7

Abstract

A jet-impactor assisted-fluidized bed (JIAFB) for continuous de-agglomeration of nanopowder agglomerates was presented in previous work. Therein, a jet caused agglomerates to impinge up an impactor, where they would break. However, efficient impactor positioning will be dictated by particle momentum: the product of solid concentration and velocity must be highest. Herein, the variation of solid hold-up was measured in a fluidized bed of Fe_2O_3 nanoparticles using gamma densitometry. Behaviour was compared under minimum fluidization and bubbling regimes, over a wide range of jet velocities (0-200 m s^{-1}). A new line-decomposition approach allowed mapping local solid distribution across seven axial and five radial positions, tangibly demonstrating how increasing the gas velocity enhanced the fluidization quality by increasing axial solid diffusivity. Conversely, increasing jet velocity locally decreased solid hold-up in the jet-affected zone, and brought about inhomogeneities. With this information in hand, jet-to-impactor distance was optimized and validated experimentally.

Keywords: nanoparticle fluidization, jet-impactor assisted fluidized bed, solid hold-up, gamma densitometry, profile reconstruction

Introduction

De-agglomeration and the production of size-controlled powders have been the focus of many studies [1-7] in powder technology applications in the pharmaceutical [8, 9], food [10], and chemical [11] industries. It becomes more important when handling cohesive powders, particularly nanopowders, in which strong interparticle forces (e.g. van der Waals forces) increase the

heterogeneity in particle size distribution through the formation of agglomerates. Common gas-based de-agglomeration methods break up dry powder agglomerates by generating a turbulent shear flow, e.g. using microjets [12-14]. Such secondary gas injection into a fluidized bed has been used in many industrial applications to control particle size [15], injecting additional reactants locally, promoting selectivity or diluting explosive reagents [16]. In previous work [17], the high kinetic energy of a jet-impactor system inside a fluidized bed was exploited to continuously and controllably break up nanoparticle agglomerates, and demonstrated experimentally that a threshold velocity (i.e. kinetic energy level) must be attained to achieve de-agglomeration. However, that study only considered particle velocity within the jet stream, ignoring the solid hold-up (the volume fraction of a flow occupied by the solid phase). While high velocity remains a requirement for agglomerate break-up, solid hold-up will dictate the overall rate at which de-agglomeration can occur – in other words, the process efficiency. Therefore, to maximize the efficiency of nanoparticle de-agglomeration, it is necessary to optimize the jet-to-impactor distance with respect to both particle velocity and solid hold-up, and this has not yet been thoroughly addressed in the literature.

In a broader view, adding a high-velocity jet changes the hydrodynamics of a fluidized bed dramatically. While different from the jet-impactor approach, several studies have shown that adding a jet to a fluidized bed system effectively enhances the fluidization performance and powder mixing within the column [12-14, 18-22] (Table 1). Hong et al. [13] investigated the effect of downward and upward jets in the fluidization of fine glass beads and fluid catalytic cracking (FCC) particles. Although their work was limited to Geldart group A powders (contrary to nanoparticles, which behave as cohesive Geldart group C particles), they concluded that a high-speed millimeter-sized jet could break the agglomerates and improve fluidization quality. Further,

a downward jet located inside the bed avoids jet penetration through the whole bed and provides more efficient solid mixing. Pfeffer et al. [12, 14], by using the same technique with single or multiple micron-sized jets, showed the jets sizes ranging from 127 to 508 μm provided enough shear to break nanoparticle agglomerates or reduce the formation of agglomerates. By measuring the bed expansion and pressure drop through the bed, they indicated that solid particles distribute in a larger segment of the bed, hence increasing the bed expansion. Dimensionless bed height measurements for a wide range of nanopowders shows microjet assistance alters the fluidization regime, from Agglomerate Bubbling Fluidization (ABF) to Agglomerate Particulate Fluidization (APF) behavior. The position of the jet has a determinant role in the performance of the bed - higher performance was achieved when the nozzle tip was close to the gas distributor plate pointing downward. In another work [21], using Focused Beam Reflectance Measurement (FBRM) and Particle Vision Measurement (PVM) probes, Pfeffer et al. characterized the number-weighted and volume-weighted agglomerate size distributions for both APF and ABF type nanopowders in the splash zone. They demonstrated that, when the superficial gas velocity increases, the concentration of agglomerates decreases, which is in fair agreement with the increased bed expansion and higher porosity observed.

To reveal the hydrodynamics of a fluidized bed in the presence of microjets, Van Ommen et al. simulated the system using a CFD-DEM model [22]. They concluded that agglomerate-agglomerate collisions are responsible for the de-agglomeration in the zone below the jet, rather than the drag force applied by the jet. In addition, their results show that voidage does not significantly change when the jet is on or off. As no bed expansion was observed in the simulation results due to the high jet speed, they further conclude that the major contribution for bed expansion comes from agglomerate breakage. Although these research endeavors have highlighted

1
2
3
4
5
6
7
8
9
10
11
12
13
14
15
16
17
18
19
20
21
22
23
24
25
26
27
28
29
30
31
32
33
34
35
36
37
38
39
40
41
42
43
44
45
46
47
48
49
50
51
52
53
54
55
56
57
58
59
60

positive effects from using jets to fluidize Geldart group C powders, the variations in solid-gas distribution patterns in the presence of jets have not yet been addressed. Understanding these dynamics is essential because the performance of multiphase systems depends significantly on the phase distribution.

Table 1 *Material and jet properties used in the literature for the fluidization of particulate materials.*

Powder	Powder Type	Jet direction(s)	Diameter of the Jet	Mach number (Jet velocity)	Objective of paper	Ref.
Glass beads	Diameter = 40 μm, Density = 2.5 g·cm^{-3} Group A	Downward and upward	2.54 cm	0.04 to 0.18 (15 to 61 m s^{-1})	Experimental and numerical study	[13]
Sand	Diameter = 421 μm, Group B	Downward jet	Downcomer size of 6 mm, opening size of 64 mm	0.015 to 0.036 (5.1 to 12.4 m s^{-1})	Hydrodynamic study	[19, 20]
Aerosil R974, 200, 90, Raw 90 (SiO$_2$) Aeroxide P25 (TiO$_2$), Alu C (Al$_2$O$_3$)	Diameter = 12-21 nm Group C (both ABF- and APF-type)	Downward and upward	127, 177, 254, and 508 μm	0.93 (320 m s^{-1})	Improving fluidization of ultrafine powders	[12, 14, 18]
Aerosil R974 (APF-type), Aerosil 90 (ABF-type)	Diameter = 12 and 20 nm Group C	Downward	Not mentioned	0.93 (320 m s^{-1})	*In situ* measurement of agglomerate size	[21]
Aeroxide P25 (TiO$_2$)	Diameter = 21 nm Group C (ABF)	Downward	128 μm	0.87 (300 m s^{-1})	Experimental and numerical study	[22]
Silica (SiO$_2$)	Diameter = 20 nm Group C (ABF)	Upward (coupled with an impactor)	254 μm	0.57 (197 m s^{-1})	De-agglomeration	[17]

The hydrodynamic properties in fluidized beds can be measured using two groups of techniques: invasive and non-invasive techniques. In invasive techniques, such as fiber optic or capacitance probes, a probe is installed inside the system and can measure phase fraction distributions locally, although this disrupts the internal flow pattern. Such disruptions are compounded in the case of cohesive powders, due to sticking on the tip of the probe. On the other hand, non-invasive techniques, such as electrical capacitance tomography (ECT), X-ray computed tomography (CT), gamma-ray tomography, and gamma-ray densitometry, generally provide information about the phase profile in a broader range such as over a line, a cross-section, or in a volume, and do not face issues related to powders sticking on the probe [23, 24]. Gamma-ray densitometry in particular is flexible, having good spatial resolution, and being suitable for a wide range of column sizes. Multi-source gamma densitometry even allows for the reconstruction of bubbles [18, 25]. Despite this, there is still a lack of simple reconstruction techniques that can assess the local phase hold-up.

Several studies have made advances to measure the solid-gas distribution, mainly using solid hold-up inside fluidized beds in the presence of jets, but not for Group C powders. The flow pattern of high-velocity gas injection into both fixed and fluidized beds was studied by Koeninger et al. [26] for fine glass beads using non-invasive particle image velocimetry (PIV) and X-ray Computed Tomography. Stimulating the bed with a horizontal millimeter-sized jet decreased the solid concentration (solid fraction of 0-3%) in the jet line, which reduced further at higher jet velocities. Hence, particle entrainment mainly occurs in the zone around the jet boundary. Moreover, no significant differences were observed for the particle velocity in fluidized and fixed states. Another non-invasive technique, gamma-ray computed tomography, was also used to measure the solid hold-up in a fluidized bed of Geldart B particles [27], showing that increasing the gas velocity not

only increases the voidage of the bed (in the core), but also improves mixing within the column, leading to more homogeneous particle fluidization. Further, the gas hold-up in the system depends on the solid particle density. The lower the particle density, the higher the voidage (i.e. lower solid phase) in the center of the bed, and a region of higher gas hold-up in the center and a region of low gas hold-up (higher solids concentration) can be determined near the walls. Koeninger et al. [26] studied particle concentration and velocity in the vicinity of a horizontal jet in a bed of glass beads (92 μm). They showed a dilute zone forms near the tip of the nozzle with a very low (1-3%) axial solid concentration, which then significantly increases and reaches a maximum corresponding to the solid concentration of the dense bed. The distance from low concentration to dense bed is translated as the jet penetration length. The solid concentration inside the jet is reduced by increasing the gas velocity. Nevertheless, the particle concentration is higher close to the nozzle tip due to the venturi effect.

Measuring the solid hold-up during nanoparticle fluidization using gamma densitometry has been the focus of a few works [23, 28]. Jiradilok et al. [28] measured the silica nanoparticle volume fraction in a circulating fluidized bed riser, showing that solid compression occurs in the riser due to pressure wave propagation following the detonation of high pressure, high temperature gas in the bed. Esmaeili and Chaouki [23] measured the solid hold-up in a fluidized bed by means of both gamma densitometry and fiber optic probing. They showed that, although bed expansion is not large enough for zirconia and aluminum nanopowders (ABF type), these fluidize uniformly in the bed. The solid hold-up in the lower part of the bed (close to the distributor) changes significantly as a function of gas velocity, whereas it remains unchanged in the upper part of the bed. This contrasts with invasive fiber optic measurements that overestimated the overall solid concentration at higher gas velocities when considering the bed expansion results.

However, adding a high velocity jet dramatically changes the hydrodynamics of a nanopowder fluidized bed, and this has not yet been addressed in the literature. Understanding the hydrodynamics of fluidized beds is key to their effective scale-up, efficient operation, and proper design. Beyond enabling to better situate an impactor for de-agglomeration, solid concentration is an important parameter to understand the agglomeration and de-agglomeration mechanisms in a fluidized bed.

In this research, the influence of a microjet flow on the solid distribution in a fluidized bed of nanopowders was evaluated in three different configurations: conventional, jet-assisted, and jet impactor-assisted fluidized bed. The axial and radial solid distribution profiles were measured for all configurations using gamma-ray densitometry, and subsequently used to reconstruct and map the local profiles. Through beam size adjustments, gamma densitometry allows focused, non-invasive measurements in the jet zone. Fe_2O_3 nanopowder was selected for this study, because of its stable long-term fluidization, increased density (i.e. lower voidage), and higher attenuation coefficient compared to other metal oxide nanopowder counterparts. With this information in hand, the jet-impactor region was focused upon to optimize the jet-to-impactor distance with respect to the impact momentum of particles and verify the optimum point with experimental force measurements. The optimized de-agglomerator can then be combined with a continuous coating process to prevent re-agglomeration [29].

Method

Principals of Gamma Densitometry

On the basis of the Beer-Lambert law, Knoll [30] showed when a beam of mono-energetic gamma

rays is propagated through a two-phase mixture, the number of photons counted per second, C, is

given by:

$$ln\left(\frac{C}{C_0}\right) = -\left[(1-\varepsilon)\left[\frac{\mu}{\rho}\right]_p \rho_p + \varepsilon\left[\frac{\mu}{\rho}\right]_g \rho_g\right]d \tag{1}$$

where C_0 is the number of photons counted per second while the system is under vacuum; ε is the

voidage of the bed; $\left[\frac{\mu}{\rho}\right]_p$ and $\left[\frac{\mu}{\rho}\right]_g$ are the mass attenuation coefficients of the solid and gas phases,

respectively; ρ_p and ρ_g are the densities of solid and gas phases, respectively, and d is the path

length of the gamma ray through the system. By neglecting the attenuation of the gas compared to

the attenuation of the solid phase, the average solid fraction in the system $(1-\varepsilon)$ along the gamma

ray line can be calculated as:

$$\varepsilon_s = 1 - \varepsilon = (1-\varepsilon_b)\frac{ln(C_g/C)}{ln(C_g/C_b)} \tag{2}$$

where subscripts s and g refer to the solid and gas and the ε_b is the voidage or porosity of the bulk

powder, which can be calculated by measuring the loose bulk density of powder (ρ_b) and particle

density (ρ_p) reported by the manufacturer:

$$\varepsilon_b = 1 - \frac{\rho_b}{\rho_p} \tag{3}$$

The loose bulk density of the powders is measured in a graduated cylinder having the same

diameter as the column (repeated three times). The graduated cylinder was filled with powders and

leveled up to a minimum height of 10 cm without compaction. The apparent density of the bulk powder is then calculated as $\rho_b = m/V$ by reading the apparent volume (V) and measuring the weight of the powder (m) with 0.1% accuracy (Table 2).

After evaluating a series of line-averaged solid hold-up values at a given height (z) and different chords (r), the cross-section solid hold-up at a given z is simply calculated by numerical integration over the cross-section based on the trapezoidal rule, assuming azimuthal symmetry. Similarly, the overall solid hold-up is calculated by integration of the cross-section solid hold-up values over the z direction.

Experimental

Materials

Magnetic iron oxide (Fe_2O_3) nanopowders, supplied by Nanostructured & Amorphous Materials, Inc. (Los Alamos, New Mexico, USA) were used for all solid hold-up experiments, owing to their ability for long-term fluidization with negligible particle entrainment, lower voidage, and high mass attenuation coefficient compared to their counterparts (e.g. silica nanopowder). Physical properties of the Fe_2O_3 nanopowders are summarized in Table 2. Very large agglomerates produced during storage, packing, and transportation were sieved out using a 40-mesh sieve with 420 μm openings before fluidization experiments. Dry nitrogen (Air Liquide 99.999 %, water content < 3 ppm) was used as both the fluidizing gas at about 40 psig (275.8 kPa) and the microjet flow at 100 psig (689.5 kPa).

Table 2 *Physical properties of powders*

Powder	Primary particle size (μm)	Particle Density (kg m^{-3})	Powder Type	Voidage*	Mass attenuation coefficient* (m^2 kg^{-1})

| Fe$_2$O$_3$ | 0.020 – 0.030 | 5240 | Geldart C/ABF | 0.78 ± 0.01 | 0.0051 ± 0.0003 |

* This data was obtained experimentally

Gamma Densitometry Tests

Gamma-ray densitometry was used to measure the solid concentration distribution in the bed and in the vicinity of the jet. A single source-detector system measured line-averaged time-averaged solid hold-up at seven axial and five radial positions, totaling 35 measurement points. The gamma densitometer consisted of a gamma-ray source, a NaI (Tl) scintillation detector (Teledyne Isotope S-1212-I), and a data acquisition system that includes a pre-amplifier, an amplifier and a discriminator (ORTEC ACE Mate) to record the signals. A scandium element (Sc 46) was used as the gamma-ray source with a half-life of 84 days, activated in the SLOWPOKE reactor at Polytechnique Montreal. For all experiments, the 450 µCi source was retained, using a two-minute total scan time for each position, as these conditions led to the lowest error measurement (~0.1%). To scan one bed cross-section, the source-detector pair, located on the opposite sides of the bed, moved along the axis perpendicular to the beam. For each cross-section, count data was collected at five chords 1 cm apart (Fig. 1). According to the jet half angle calculations [31], the collimator was designed such that the spatial resolution of the gamma densitometer is 2 mm at the bed center line (e.g. at the tip of the nozzle), calculated based on the collimator configuration parameter [25, 32]. This guarantees the entire beam is within the jet zone. Additional details pertaining to the gamma-ray densitometry approach are provided as supplementary information (Fig. S1,2).
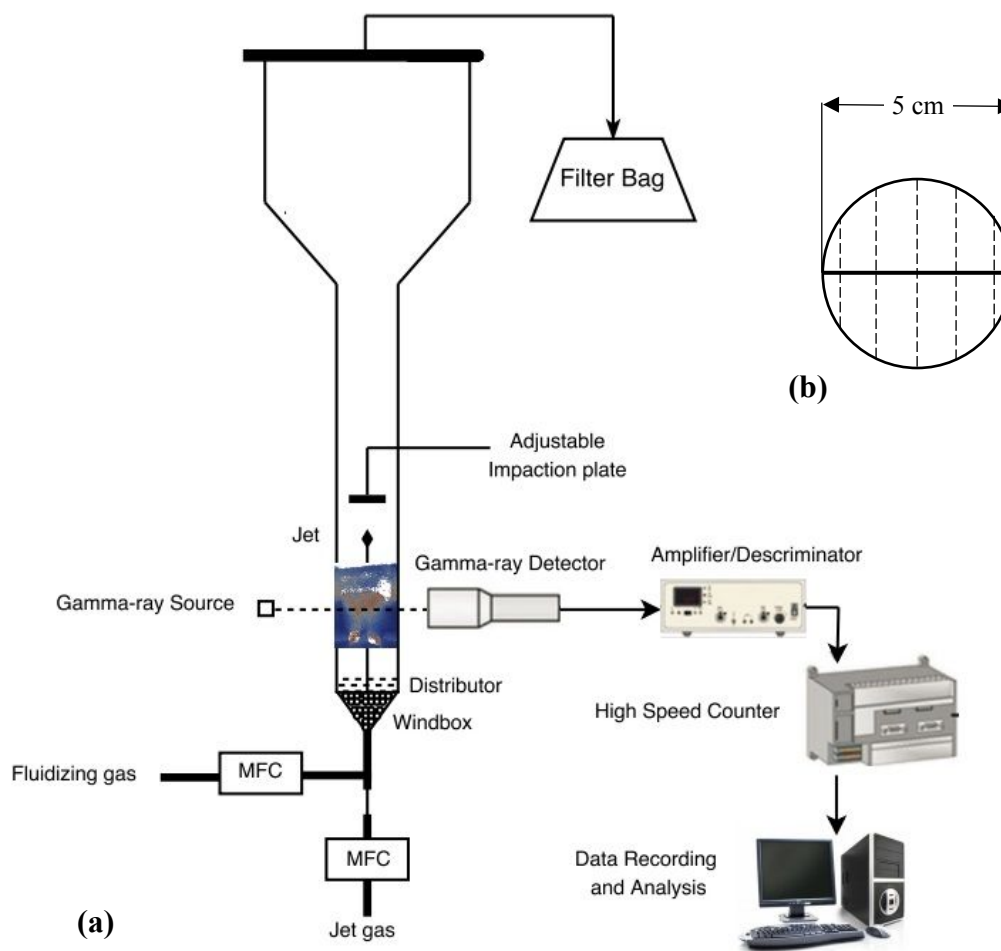
Figure 1 *(a) Schematic of the fluidized bed and gamma-ray densitometry system; (b) Five radial positions (chords) to map solid hold-up in a column cross section*

Experimental Setup

The fluidization column consisted of a poly(methyl methacrylate) (Plexiglas) tube with an internal

diameter of 0.05 m and a wall thickness of 0.007 m (Fig. 1). The total height of the bed and

freeboard was 60 cm, and it was connected to a larger cylinder with a diameter of 0.3 m, used as

the disengagement zone. This prevented the particles from being entrained out of the bed by

decreasing the upward flux of particles and gas. Several ports at different heights allowed for the

installation of the microjet and the impactor plate. The fluidizing gas, after passing through a mass

flow controller (MFC), wind box, and distributor with a pore size of 20 μm entered the column.

The wind box contained small wood packings to uniformly distribute the gas flow. A 0.01 inch (254 μm) ID upward tube was employed as the jet, and the jet flow was controlled by a second mass flow controller. At the end of the disengagement zone, a HEPA filter bag removed any entrained nanoparticles. Two pressure ports, at the top of the distributor and at the top of the freeboard, were connected to a digital manometer to measure the differential pressure across the bed.

Force Measurements

A commercial piezoresistive force sensor (Honeywell Sensing and Productivity Solutions) was adapted to measure forces applied from the gas and solid particles inside the jet flow. The input voltage was maximized (12 V) to make the sensor more sensitive to the jet flow. The measuring surface of the sensor was extended by gluing a very thin, 1-inch stainless-steel disc on top of its actuator. The force sensor assembly was then attached to a stainless-steel rod and the electronic pins and connections were covered, without touching the actuator, to avoid any damage or errors resulting from nanopowder ingress. The force sensor was calibrated using standard calibration weights before the tests (Fig. S6). The assembly was installed within the fluidized structure such as to allow only vertical displacement without diverging horizontally. The output signal from the sensor was recorded using a data acquisition card connected to a computer. Each data point was recorded over two minutes at a sampling frequency of 10 Hz, and all measurements were repeated three times.

Results and Discussion

Fluidization behavior of iron oxide nanopowder and overall solid hold-up

Theoretically, 20 nm magnetic Fe_2O_3 nanoparticles, due to their size and density, should be fluidized individually at very low superficial gas velocities, on the order of 10^{-7} cm/s. However, experiments show the onset of fluidization occurs at a gas velocity of 0.85 cm/s (Fig. 2), which corresponds to the fluidization of a 70 μm particle (assumed density of 1150 kg/m^3) [33]. This significant difference demonstrates that nanopowders are fluidized in the agglomerate state due to the high level of interparticle forces present, mainly van der Waals interactions. At 0.85 cm/s, Fe_2O_3 nanopowders begin to fluidize uniformly with a low bed expansion (10% of initial height of the bed). Expansion increase to 55% of initial bed height at superficial gas velocities three times larger than minimum fluidization velocity (U_{mf}) (Fig. 2). The onset of the bubbling regime occurs at a gas velocity of 1.7 cm/s. Bubble size increases with gas velocity up to 3 cm/s, which may cause negligible elutriation in long-term fluidization. These characteristics, along with the physical properties of the powder (i.e. simple agglomerate size and bulk density), indicate an ABF regime according to the Wang sub-classification [34], in agreement with previous works [35]. As a rule of thumb, nanoparticles (< 100 nm) with a bulk density > 100 kg m^3 are fluidized as ABF, whereas those with a bulk density < 100 kg m^3 show an APF behavior [34]. In the presence of the nozzle, the bed expansion increases by a maximum of 5 % at the highest jet velocity (i.e. 200 m/s), confirming that the upward nozzle does not change the fluidization behavior of the nanopowders.
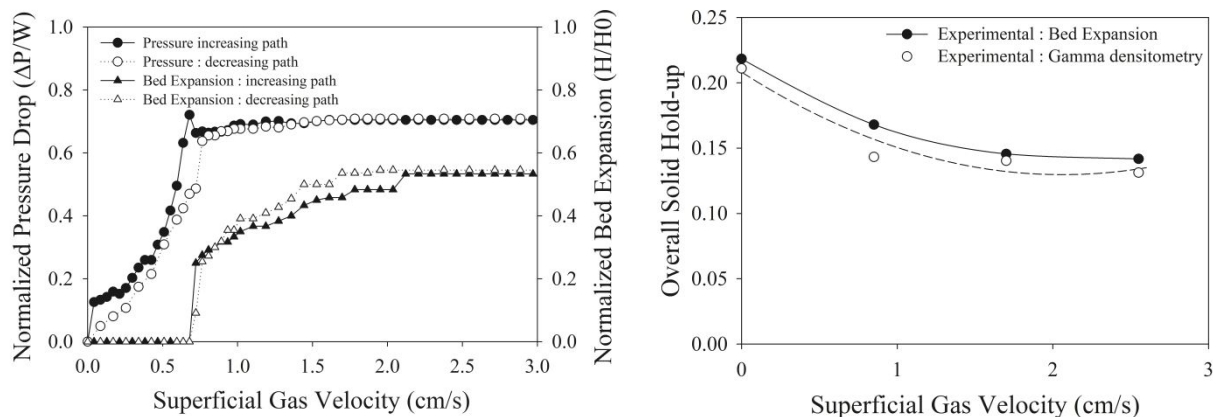
Figure 2 *(a) Fluidization curve for iron oxide nanoparticles; (b) comparison of overall solid hold-up measurements using bed expansion results and improved gamma densitometry.*

Before evaluating solid hold-up in the presence of a jet and an impactor, the results, obtained from gamma densitometry, were first verified with the overall solid hold-up results obtained based on the bed expansion measurements. The latter calculates the overall solid hold-up based on the simple mass balance of the uniformly distributed solid powder in the fluidized bed assuming no elutriation. Given that, experimental bed expansion data can provide a rough estimation of the overall solid hold-up over a wide range of superficial gas velocities. Fig. 2b compares the calculated overall solid hold-up from both measurements, confirming that it follows the same trend with a maximum solid hold-up error of 2%, which may stem from the bed expansion measurements and rough assumptions in calculating solid hold-up values. This gives confidence to move forward and study the local solid hold-up in other zones, particularly in the vicinity of the jet, which is not possible to be measured using the bed expansion measurement.

Radial solid hold-up

To study the effect of the microjet and microjet-impactor on the fluidization behavior of Fe_2O_3 nanopowders, a series of experiments were performed over a wide range of jet velocities (0-200 m/s) in three configurations: conventional (unassisted) fluidization, fluidization in the presence of the jet, and fluidization in the presence of both the jet and the impactor. Count data was registered

for 2 minutes with a sampling time of 10 ms, leading to 12,000 data points per measurement. In order to study the solid hold-up in the vicinity of the jet, the gamma densitometer scanned the bed 2.5 mm above the nozzle tip.

Conventional fluidization Typical fluidization, without installation of a jet, shows a uniform radial solid phase distribution (Fig 3a and 3b). In the axial direction, the solid phase is more concentrated at the bottom of the bed, and more diluted in the upper sections. At U_{mf}, as the bed has not yet fully expanded, a very dilute zone is detected in the splash zone (15 cm above the distributor). By increasing the superficial gas velocity up to three times the minimum fluidization velocity, the bed becomes fully uniform, and the solid phase distribution increases at 15 cm above the distributor, due to full bed expansion (Fig. 3b). As expected, the cross-section solid hold-up values decrease with rising gas flow in the system.
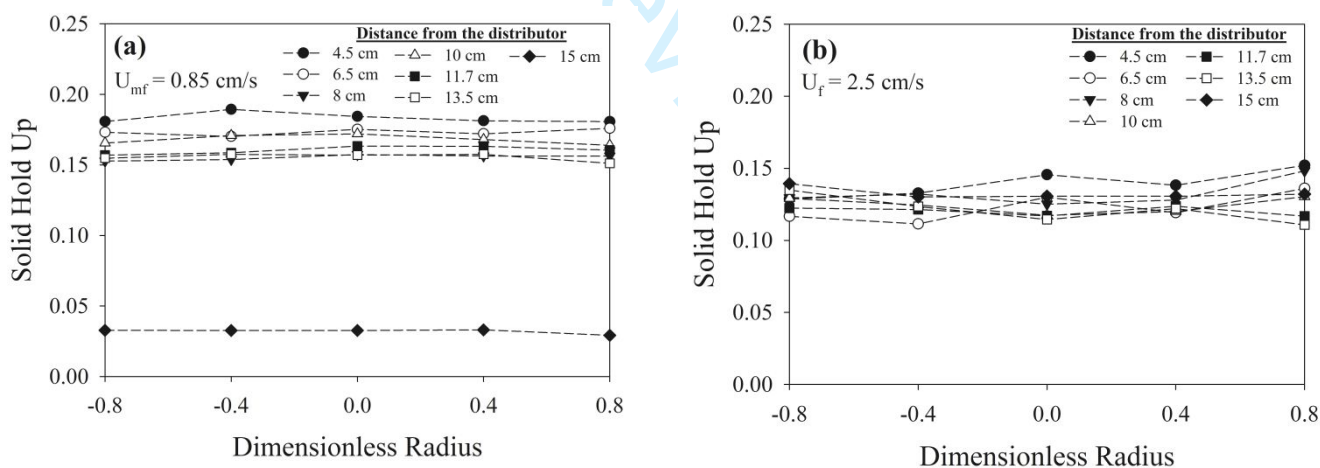
Figure 3 (a) Radial solid hold-up at seven levels above the distributor for the conventional fluidization at (a) minimum fluidization (U_{mf} = 0.85 cm s^{-1}), and (b) bubbling regime (U_f = 2.5 cm s^{-1})

Microjet-assisted fluidization Once the jet is turned on at U_{mf}, the solid hold-up locally drops at 2.5 mm above the nozzle tip ($r/R = 0$), while it remains almost constant at other radial positions (Fig. 4a). The local solid hold-up reduction is more evident at higher jet velocities, representing the formation of a "hole" inside the fluidized bed. This is reasonable as more gas is injected to the

system, the less solid hold-up is observed. Comparing the solid hold-up profiles of zero and non-zero jet velocities, injecting the secondary gas stream causes reduction of the mean cross-section solid hold-up in the vicinity of the jet. However, in the bubbling regime (Fig. 4b), this local jet effect becomes less apparent. Although the mean cross-section solid hold-up drops compared to the U_{mf} regime because of dilution, the solid hold-up profiles remain almost uniform, while at jet velocities greater than 100 m s^{-1} the jet effect becomes detectable. The results for both regimes show increasing the fluidization gas flow diminishes the effect of the secondary gas flow as a result of increasing bubbles in the system. These alter the flow pattern, thereby increasing mixing and uniformity in the system. Nevertheless, the void created by the microjet is still detectable when the volumetric flow rate of the jet is at least 10% of the superficial gas velocity. This agrees with previous studies for group B and D particles showing that an increase in superficial velocity, exceeding U_{mf}, results in shorter jet lengths [36-39].
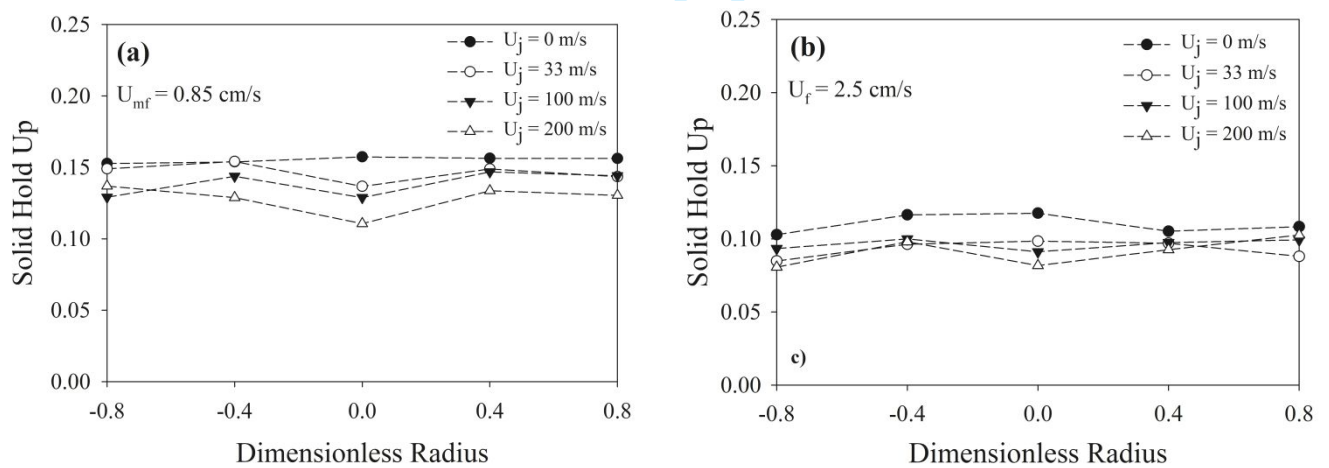
Figure 4 *Radial solid hold-up profile for microjet- assisted fluidization at (a) minimum fluidization velocity (U_{mf} = 0.85 cm s^{-1}), and (b) bubbling regime (U_f = 2.5 cm s^{-1}). Jet is centered at dimensionless radius 0.0.*
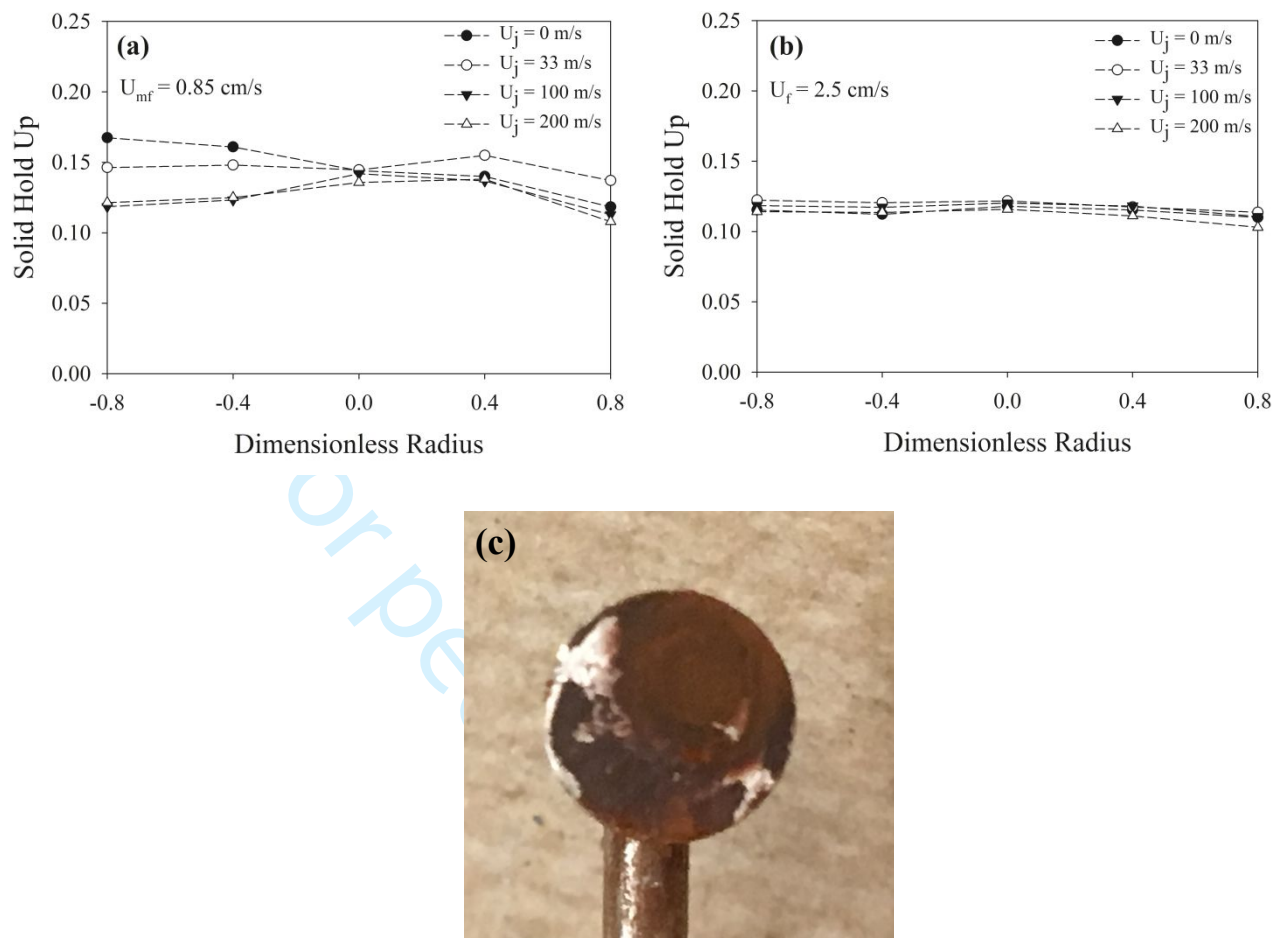
Figure 5 Radial solid hold-up profile for microjet-impactor-assisted fluidization at (a) minimum fluidization velocity (U_{mf} = 0.85 cm s^{-1}) and (b) bubbling regime (U_f = 2.5 cm s^{-1}); (c) the image of impaction plate after the test.

Microjet-impactor assisted fluidization Installing the impactor causes the solid hold-up profiles to become asymmetric in the vicinity of the microjet-impactor (Fig. 5a and 5b). In the U_{mf} regime, once the jet is off ($U_j = 0$ m s^{-1}), solid hold-up increases slightly from 15% to 17% at the side of the column where the impactor arm is mounted, while it decreases from 15% to 12% at the other side of the column. This occurs due to the side-mounted impactor's arm hindering the free flow of gas. When starting the jet stream, two different phenomena are observed depending on the jet velocity. At lower jet velocity ($U_j = 33$ m s^{-1}), solid hold-up slightly reduces under the impactor arm, while it rises under the free section. However, by increasing the jet velocities beyond 100 m s^{-1}, this flow pattern changes. The mean cross-section solid hold-up drops, and this reduction is

more significant under the impactor arm. The jet penetration length calculations based on the

Hirsan correlation [36] explains this difference in flow patterns in the vicinity of the microjet-

impactor (Table 3). Since the distance between the nozzle tip and the impaction plate is 5 mm, at

lower jet velocities the maximum jet penetration length is not sufficient to reach to the plate, hence

jet flow entrains some particles, splashing them around. However, at jet velocities exceeding 100

m s^{-1}, the jet length reaches the impactor plate and, due to gas reflection, the solid hold-up drops

noticeably at non-centered radial positions. The profile is asymmetric since the impactor has not

been installed exactly perpendicular to the jet. Inspecting the impactor after the test confirms this

(Fig. 5c). This latest result emphasizes that the parametric study (in supplementary information)

improved the densitometry efficiency enough to make this measurement technique sensitive to a

slight deviation in jet-impactor installation.

Table 3 Minimum, maximum and bubble penetration length as a function of gas jet velocity based on Hirsan correlations [36] for an upward nozzle

Gas Jet Velocity (m s^{-1})	Minimum jet penetration length (mm)	Maximum jet penetration length (mm)	Jet bubble penetration length (mm)
33	0.6	2.6	4.5
100	1.1	6.2	10.1
200	1.9	11.1	16.1

Local Solid hold-up in the vicinity of the jet

Unlike the capacitance probe or fiber optic methods used for characterizing local parameters in

previous works, gamma densitometry measures solid phase concentration based on the line-

averaged attenuation of the gamma ray travelling through the system. Although the line-averaged

solid hold-up provides information about how the radial and cross-sectional solid particle

distribution varies at the jet level as a function of the jet or fluidization velocity, it does not describe the local solid phase distribution in the vicinity of the jet, due to the inherent averaging of the gamma-densitometry technique. In other words, the contribution of secondary gas flow (jet) to solid hold-up distribution is diminished in the fluidizing gas flow. To overcome this problem, a line decomposition approach is proposed to isolate the effect of the secondary microjet flow on the solid hold-up, assuming the solid hold-up is uniform far enough from the jet affected zone (JAZ). For this purpose, the bed is first divided in a number of rings (Fig. 6), such that each radial position is allocated to a ring. Next, the solid hold-up needs to be estimated in the outer ring. In the previous section, it was shown Fe_2O_3 nanoparticles fluidize homogenously far away from the jet zone, whereas in the vicinity of the jet the local solid phase concentration changes noticeably due to turbulence. Koeninger et al. [26] showed that, in fluidization of solid particles, solid concentration varies in the jet boundary, where the phase and momentum exchange takes place. Consequently, it is fair to assume that the local solid hold-up is uniform in azimuthal angles far from the JAZ (i.e. in the outer ring). Here, since solid hold-up was measured at five points at each cross section, the surface area is decomposed at each level into three zones (Fig. 6). Hence, it may be assumed that:

$$\varepsilon_{l_3} = \varepsilon_r|_{\frac{r}{R} = \pm\, 0.8} \tag{4}$$

where, ε_{l_i} and ε_r are the local and radial solid hold-up, respectively. Decomposed solid hold-up values are referred to herein as "local solid hold-up", representing the solid hold-up values in each ring. Generally, solid concentration in fluidized beds varies in all dimensions:

$$\varepsilon_s = \varepsilon_s(r,\theta,z) \tag{5}$$

At a given height (z) by assuming an azimuthal symmetry as a result of uniform solid distribution, the correlation can be simplified to,

$$\varepsilon_s = \varepsilon_s(r) \tag{6}$$

Combining this with the Knoll variant of the Beer-Lambert law (Eq. 1) considering a constant mass attenuation coefficient gives:

$$A = ln\left(\frac{C}{C_0}\right) \sim \varepsilon_s(r).d \tag{7}$$

On the other hand, the total linear attenuation (A) is the sum of its constituents (i.e. individual interactions of the gamma ray with the solid phase in the ith zone, A_i),

$$A = \sum_{i}^{n} A_i(r) \tag{8}$$

Therefore, the time-averaged local solid hold-up at any elevation and radial position is derived from the radial solid hold-up value, by neglecting the non-linear average error in space (acceptable due to the small size of the gamma beam):

$$\varepsilon_r\big|_{\frac{r}{R}} = \frac{1}{d}\sum_{i}^{n} \varepsilon_{l_i} d_i \tag{9}$$

where ε_r is the radial solid hold-up at a given r/R, ε_{l_i} are the local solid hold-up of ith zone, d and d_i are the distance which gamma-ray travels in that radial position and in the ith zone, respectively.
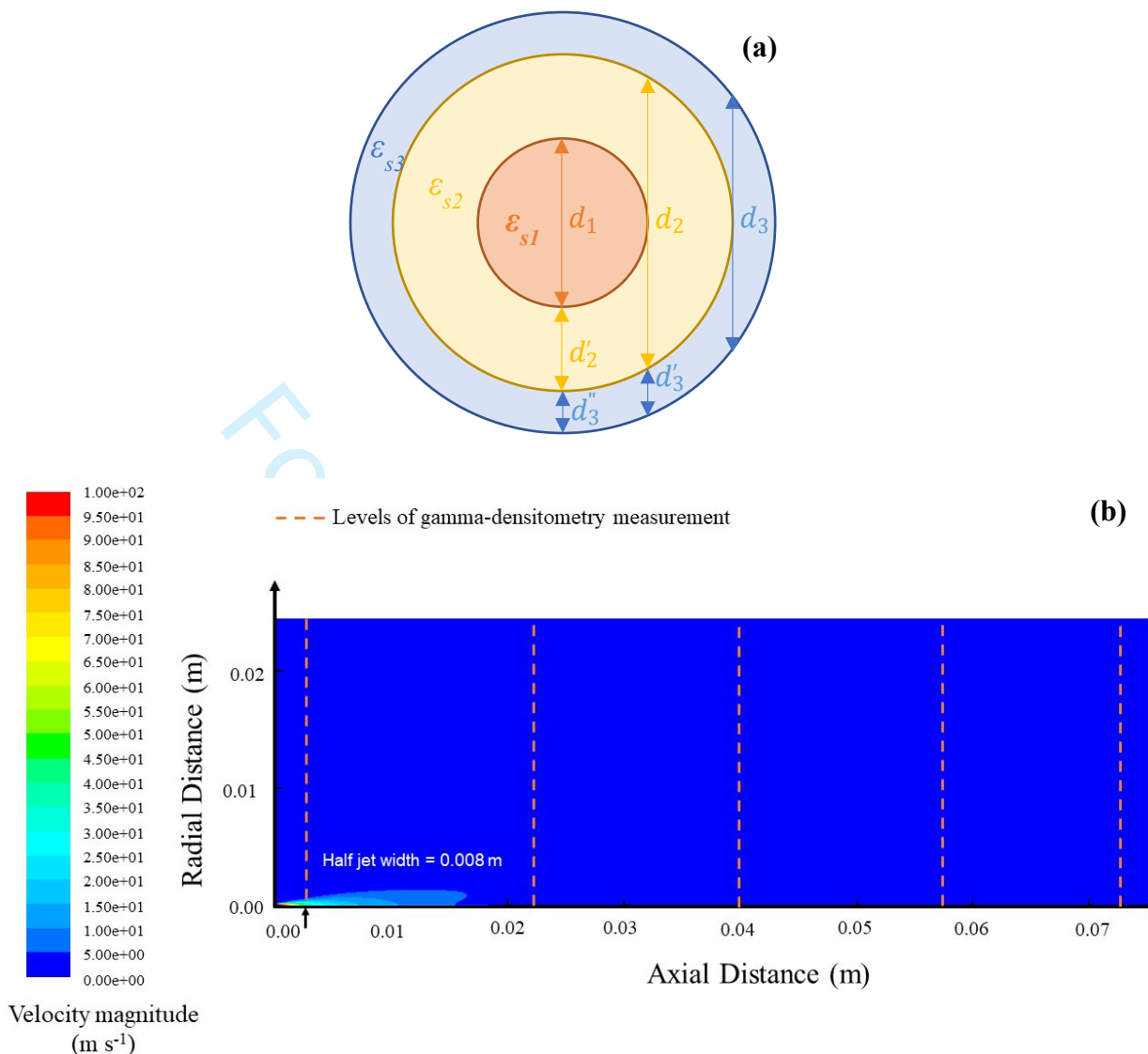
Figure 6 *(a) Top view of the column showing decomposition of line-averaged solid hold-up; (b) measurement levels overlaid on gas velocity contour obtained by simulation in Fluent to determine the width of JAZ at U_f = 2.5 cm s^{-1} and U_j = 100 m s^{-1}*

To determine the extent of the JAZ (d_1 in Fig. 6), a single-phase simulation was performed for all superficial gas and jet velocities using the Fluent 6.3 CFD software. The assumptions and model have been discussed in detail in previous work [17]. By simplifying the model to a two-dimensional axisymmetric case, the geometry was defined as a 5 cm by 60 cm rectangle. A 127 μm line was defined as the tip of the nozzle. Nitrogen was selected as a compressible fluid flow medium. The model was run for two fluidizing gas velocities (0.85 and 2.55 cm s^{-1}) and three jet velocities (33, 100, and 200 m s^{-1}). k-ε turbulent physics were used for the case of stationary

studies, due to the high Reynolds numbers of the jet (3 to 8×10^3). Although the simulation does not account for the motion of particles, it serves as an approximation to determine the jet widths based on the gas velocity field. The jet width at each cut plane was defined as the position at which the gas velocity reduces to a cut-off point of 5% of the maximum velocity magnitude at the given level. The calculated jet width values show that changing the fluidization regime does not affect the jet width. The half jet width values for all runs show a constant value of 0.008 m at 2.5 mm above the nozzle tip. Since the maximum jet penetration length according to this model and Hirsan correlations (Table 3), even at the highest velocity, does not reach to the second gamma densitometry measurement level, the minimum size of the central zone (d_1) was kept constant at 1 cm during line decomposition. Ultimately, 3D solid hold-up profiles are plotted at seven heights combining the jet widths obtained from this simulation and local solid hold-up values obtained from Eq. 9 (Fig. 7, 8). These figures reveal the locations at which the solid hold-up is reduced and/or increased by the microjet. At U_{mf} (and $U_j = 0$ m s^{-1}), solid hold up is increased near to the bottom of the bed, while it becomes more diluted at higher levels. At the highest level (15 cm above the distributor, the splash zone), the solid concentration is almost zero as the bed has not yet fully expanded. By turning on the jet to $U_j = 33$ m s^{-1} (Fig. 7b), the solid hold-up reduces close to the distributor because part of the bed is being carried by the microjet flow. Moreover, a very low solid concentration zone is being formed at 2.5 mm above the tip of the nozzle, due to the injection of the secondary gas flow. However, the jet penetration length is not sufficient to affect the local solid hold-up at higher levels. By increasing the jet velocity to $U_j = 100$ and 200 m s^{-1} (Fig. 7c,d), the solid hold-up in the center noticeably reduces not only at the jet level, but even at higher levels since the jet penetration length rises. At the maximum jet velocity ($U_j = 200$ m s^{-1}), the total flow (i.e. fluidizing gas and microjet flow) is high enough to expand the bed to the level of measurement.

Also, at all jet velocities, a concentrated zone is identified right under the jet, which indicates
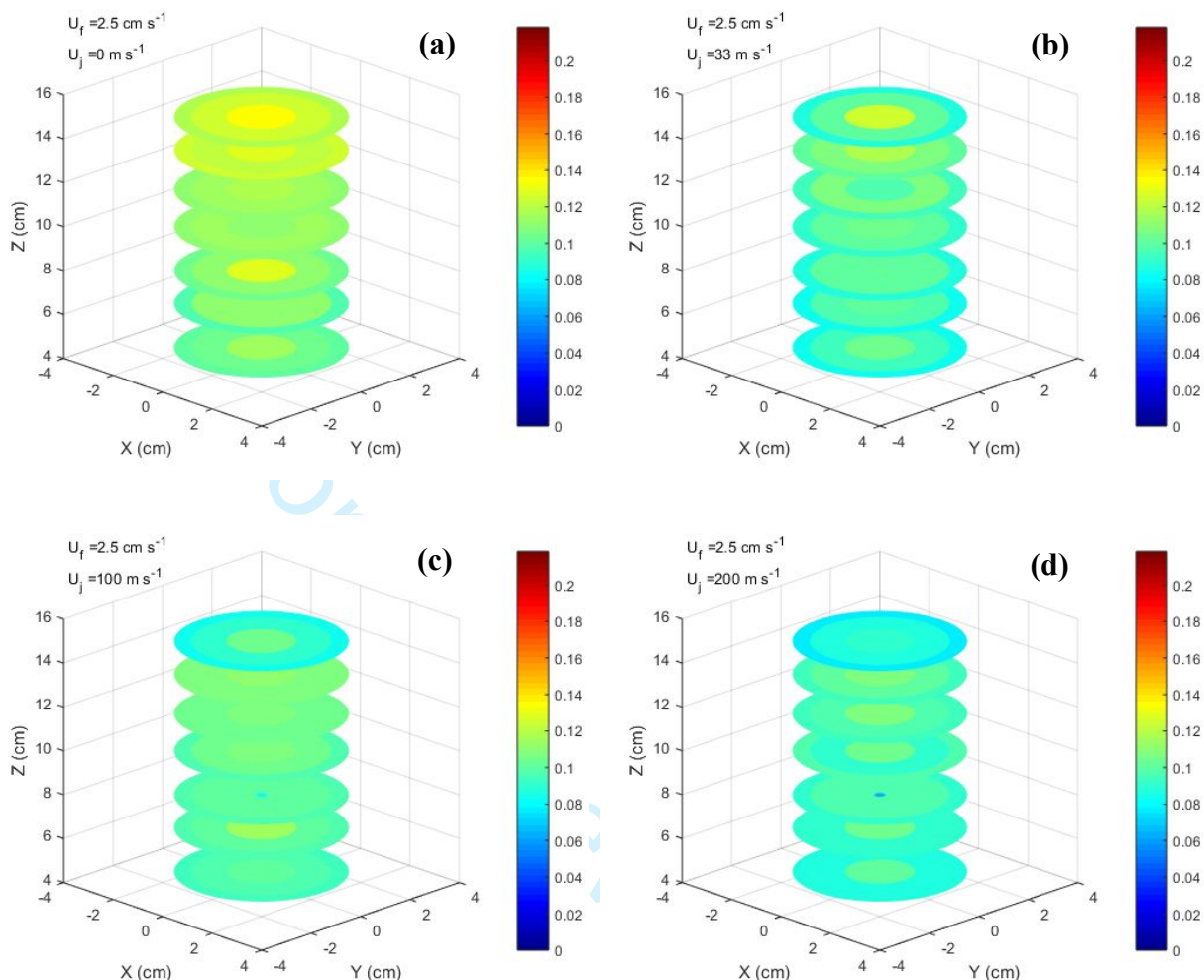
formation of a dead-zone under the microjet tube.
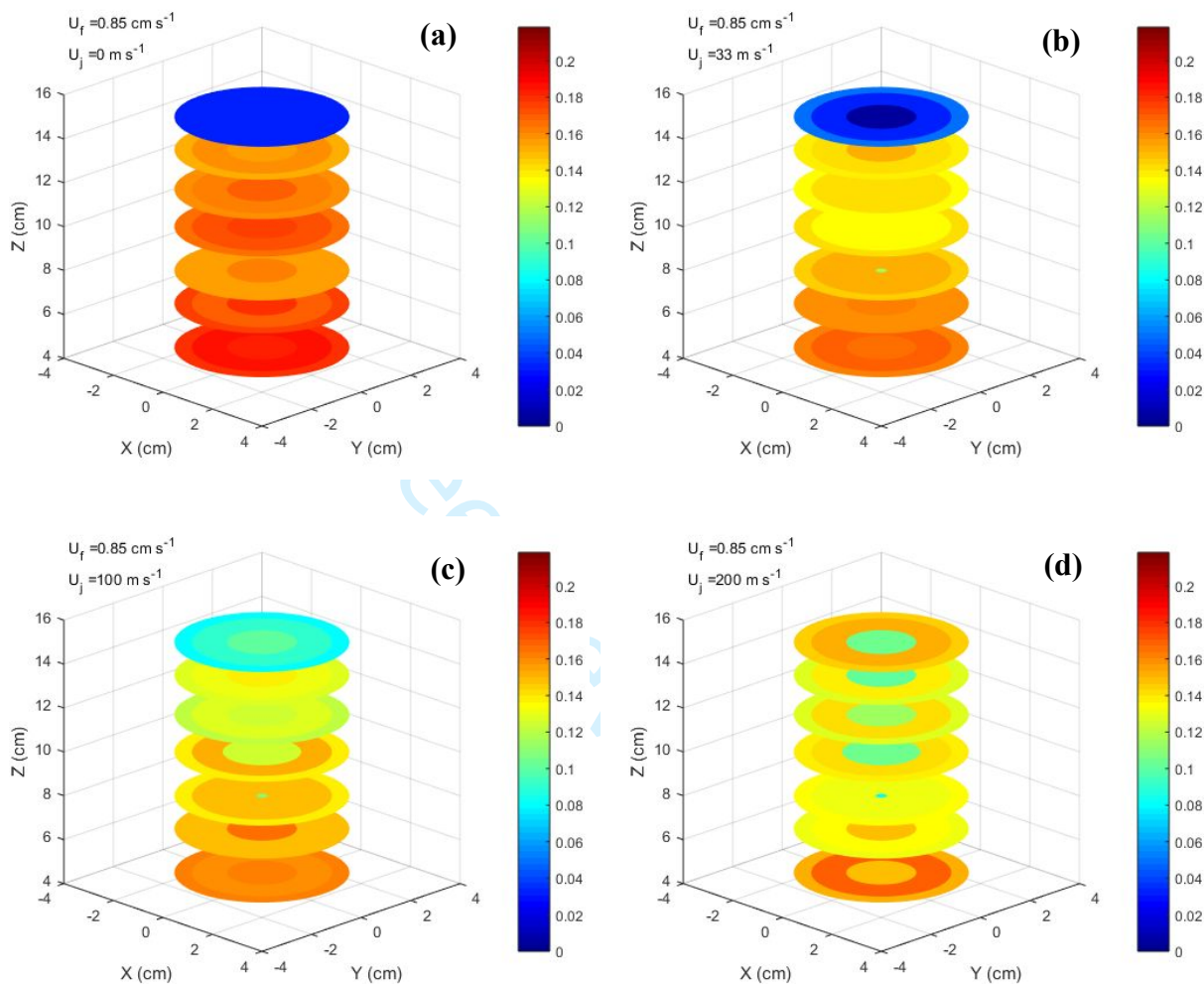
Figure 7 *(a) 3D local solid hold-up profiles at seven cross sections calculated by line-decomposition approach at*
U_{mf} = 0.85 cm s^{-1}, U_j = 0; (b) U_j = 33 m s^{-1}; (c) U_j = 100 m s^{-1}; (d) U_j = 200 m s^{-1}

By changing the fluidization regime to bubbling (U_f = 2.55 cm s^{-1}) (Fig. 8), the axial solid

diffusivity enhances so the solid hold-up through the bed is more homogeneous compared to the

minimum fluidization regime. Ettehadieh et al. [40] previously showed a centimeter-sized jet

makes the axial solid hold-up uniform for Geldart D particles by increasing the solid diffusivity in

this direction. However, since the radial solid diffusivity is constant for small bed diameters [41],

the bed remains almost uniform in the radial directions at all gas velocities. In this regime, the

general patterns of solid hold-up variations identified at U_{mf} remain, but at proportionally lower solid hold-up values as a result of introducing more fluidizing gas to the system. At this increased fluidization velocity, jet effects are reduced (Fig. 7 vs. Fig. 8). In the bubbling regime, the dilute zone in the jet is no longer detectable at low U_j (Fig. 8b), while it starts developing by increasing U_j to 100 and 200 m s^{-1} (Fig. 8c,d). However, the jet penetration length at U_j = 100 m s^{-1} is still too short to influence the local solid hold-up at higher levels. Eventually, at U_j = 200 m s^{-1} (20 v% of the fluidizing gas flow), the maximum jet penetration length increases. Thus, discharged bubbles from the jet can travel further and consequently reduce the local solid hold-up at higher levels (Fig. 8d).

In a broader view, these solid hold-up profiles clarify how, in both regimes, the microjet improves the fluidization quality of nanoparticles and affects the solid hold-up distribution throughout the bed, despite their local inhomogeneities. This is essential since it enhances mass and heat transfer performance inside fluidized beds. Comparing the local solid hold-up profiles when the jet is off and on (Fig. 7a,b and Fig. 8a,b) indicates the axial distributions of solid particles have been enhanced. This occurs as a result of overcoming interparticle forces, which in turn leads to breakage of nanoparticle agglomerations [14, 22] and increased total gas flow. The higher the jet momentum, the higher the axial solid diffusivity, and thus the more homogeneity in the bed. While this was expected intuitively, the improved gamma densitometry technique has tangibly demonstrated and quantified local solid hold-up, showing how a given constant local phenomenon (such as a jet) can directly impact solid/gas phase distribution.

Figure 8 *3D local solid hold-up profiles at seven cross sections calculated by line-decomposition approach at U_f = 2.5 cm s⁻¹. (a) U_j = 0 m s⁻¹; (b) U_j = 33 m s⁻¹; (c) U_j = 100 m s⁻1; (d) U_j = 200 m s⁻¹*

Optimizing the jet-to-impactor distance

Solid hold-up along the jet axis

The determination of local solid hold-up values (ε_l) along the jet axis at U_j = 100 m/s and U_f = 2.5 cm s⁻¹ was made possible by the line decomposition approach presented in the previous section. Fig. 9a illustrates that solid hold-up increases sharply from the nozzle tip (where particle hold-up is zero) up to 7.8% at 0.0025 m above the nozzle tip. At ca. 0.02 m above the tip, it has reached its final value of approximately 10.5%. This is in general agreement with the jet length values calculated by Hirsan [37] (Table 3), that show that, at U_j = 100 m s⁻¹, the JAZ

extends to 0.0011 m (up to 0.0062 m). After this JAZ, the jet loses its form and turns into high-momentum bubbles. In the early section of the JAZ, solid particles are dragged into the jet stream as a result of negative pressure generated via the high-speed jet. Moving away from the nozzle tip, more and more particles are entrained into the jet flow until the end of JAZ is reached, at which point solid hold-up remains constant as the jet no longer affect the solid distribution in the bed.
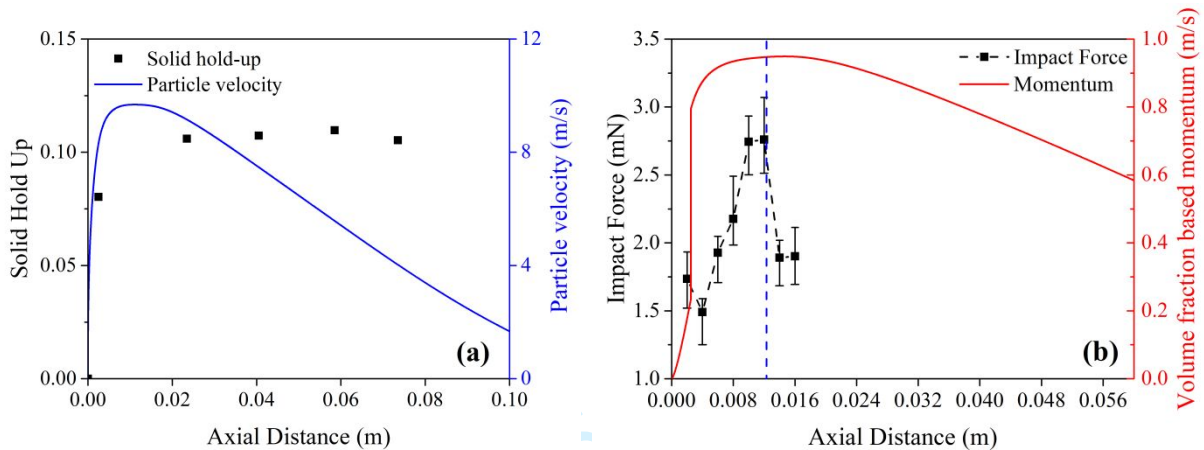
Figure 9 (a) *local solid hold-up profile as a function of axial distance to the nozzle tip (black data points) and velocity of particles with the average size of 70 μm (blue curve); (b) Impact force profile (black data points, error bars show the absolute error) and momentum profile of impacted particles as a function of axial distance to the nozzle tip*

Particle velocity

The velocity of fluidized particles in the vicinity of the high-velocity jet was obtained by a two-way coupling simulation using the Fluent 6.3 CFD software (same geometry as simulations used to calculate jet width in the previous section). The fluidized particles were considered as nanoparticle agglomerates with a diameter of 70 μm. k-ε turbulent model was used in combination with wall functions for the continuous gas phase. For the dispersed phase, particle motion is obtained by integrating the force balance. To simplify, only three hydrodynamic forces were considered (drag, buoyancy and gravitational forces) and were written in a Lagrangian frame on the particles. In the set of differential equations that calculate particle velocities and positions, heat and mass transfer are neglected, and particles are assumed to be spherical. In a two-way approach,

the velocity field calculated via the Reynolds-averaged Navier–Stokes (RANS) equations is used to solve dispersed phase motion equations. The calculated dispersed phase momentum is then used to update the velocity field of the continuous phase. However, particle-particle interactions are neglected. After solving the equations, a mesh and particle study was performed to ascertain that the injection point of particles and the mesh size did not affect the solution of the model (Fig S3-S5).

Fig. 9a (blue curve) shows the velocity of particles that were entrained and accelerated by the jet flow. The particles rapidly accelerate from their initial fluidization velocity of 2.5 cm s^{-1} and reach their maximum value (10 m s^{-1}) approximately 0.012 m from the tip of the nozzle. The particles then gradually slow down under the effect of gravity until they reach the superficial velocity in the column. Combining the solid hold-up and velocity yields the particle momentum curve (Fig. 9b, red), which reaches its apex at approximately 0.012 m above the tip of the nozzle. Thus, for $U_j =$ 100 m s^{-1} and $U_f =$ 2.5 cm s^{-1}, this is the optimum point to place an impactor in a jet-impactor system. Extending beyond this specific case, the general rule of thumb would be:

- If the jet penetration length is smaller than the point at which maximum particle velocity is reached, the jet penetration length can be retained as the optimal position to install an impactor;
- If the jet penetration length is greater than the point at which maximum particle velocity is reached, the point of maximum particle velocity can be retained as the optimal position for an impactor.

Force measurement tests

To validate the impactor position recommendation (0.012 m), the local force resulting from the impact of jet flow and accelerated particles on the impactor was measured at different jet-to-

impactor distances. For this purpose, a force sensor was placed within the bed, perpendicular to

the jet flow.

Fig. 10 illustrates the force signals recorded at U_f = 2.5 cm s^{-1} and U_j = 100 m s^{-1} at axial distances

of 2, 6, 10 and 14 mm from the jet. The values shown result from the application of a moving

average filter with a window size of 20 seconds. The raw signal, noisy from random high frequency

collisions, is provided in supplementary information. The force difference between sections where

U_j = 0 and U_j = 100 m s^{-1} is considered as the force applied by the jet flow (F_j).
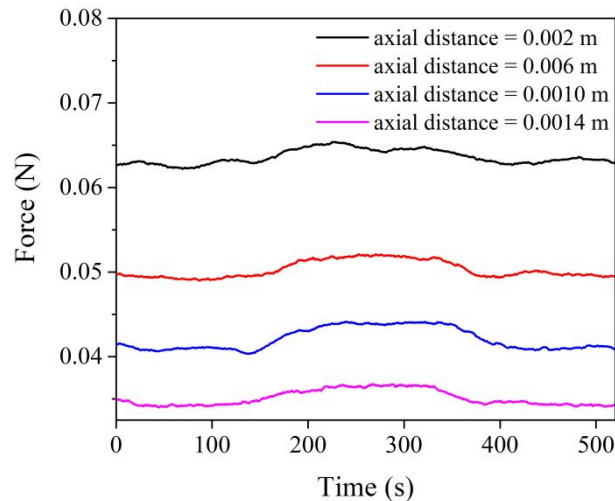
By measuring F_j at eight different axial distances, the jet flow force profile is obtained (Fig. 9b).

In agreement with the overlaid momentum curve, F_j increases in the axial direction and reaches

its maximum ca. 0.012 m from the tip of the nozzle.

Concluding Remarks

The influence of a microjet and microjet-impactor on the fluidization of Fe$_2$O$_3$ nanopowder under

two fluidization regimes (minimum fluidization and bubbling) and a wide range of jet velocities

(0-200 m s^{-1}) was studied using gamma densitometry, and compared with conventional fluidization. In conventional fluidization, a uniform radial solid phase distribution was observed, which was more concentrated at the bottom of the bed. By increasing the jet velocity, the solid hold-up locally drops more and more at the center, forming the JAZ. Adding an impactor against the jet changes the previous symmetric profile to an asymmetric profile due to gas reflection and the impedance of gas by the side-arm mount of the impactor.

To spotlight the JAZ, a line-decomposition approach was proposed to reconstruct the 3D local solid hold-up profile based on the radial solid hold-up values. Local solid hold-up maps showed that, under the minimum fluidization regime, solids are not well distributed axially, while this becomes more homogeneous in transition to the bubbling regime. However, increasing the jet velocity at a given regime locally varies the solid phase distribution along the jet axis as a result of injecting extra gas and causes local inhomogeneities. Further, increasing the fluidizing gas velocity diminishes the jet effect, likely by reducing the jet length.

Finally, the local solid hold-up profile along the jet axis was combined with a particle velocity profile, provided by a two-way CFD simulation, to optimize the jet-to-impactor distance and thus maximize the impact momentum. The highest momentum point occurs at 0.012 m above the tip of the nozzle for U_f = 2.5 cm s^{-1} and U_j = 100 m s^{-1}. This optimum point was then validated experimentally using local force measurements along the jet axis.

This study provides insights for the proper design and scale-up of the jet-assisted fluidized bed reactors particularly for nanopowders, including cases where an impactor is used. Further, it provides a methodology for subsequent solid hold-up tests (detailing an improved gamma densitometry technique in supplementary information, and a new line deconvolution approach),

and provides guideline to maximize the impact momentum when agglomerate breakage is required.

Acknowledgments

Literature Cited

[1] S. Pradhan, J. Hedberg, E. Blomberg, S. Wold, I. Odnevall Wallinder, Effect of sonication on particle dispersion, administered dose and metal release of non-functionalized, non-inert metal nanoparticles, Journal of Nanoparticle Research, 18 (2016) 285.

[2] V. S. Nguyen, D. Rouxel, R. Hadji, B. Vincent, Y. Fort, Effect of ultrasonication and dispersion stability on the cluster size of alumina nanoscale particles in aqueous solutions, Ultrasonics Sonochemistry, 18 (2011) 382-388.

[3] H. Yoden, N. Itoh, Effect of Small Size Beads on Dispersion of Nanometer-Sized Silica Particle by Wet Beads Mill Process, Journal of the Society of Powder Technology, Japan, 41 (2004) 457-464.

[4] M. Inkyo, T. Tahara, Dispersion of Agglomerated Nanoparticles by Fine Beads Mill, Journal of the Society of Powder Technology, Japan, 41 (2004) 578-585.

[5] Y. Hwang, J. K. Lee, J. K. Lee, Y. M. Jeong, S. I. Cheong, Y. C. Ahn, S. H. Kim, Production and dispersion stability of nanoparticles in nanofluids, Powder Technology, 186 (2008) 145-153.

[6] J. A. Kurkela, D. P. Brown, J. Raula, E. I. Kauppinen, New apparatus for studying powder deagglomeration, Powder Technology, 180 (2008) 164-171.

[7] M. Seipenbusch, P. Toneva, W. Peukert, A. P. Weber, Impact Fragmentation of Metal Nanoparticle Agglomerates, Particle & Particle Systems Characterization, 24 (2007) 193-200.

[8] W. H. Finlay, Ch. 9: Dry powder inhalers, in: W.H. Finlay (Ed.) The Mechanics of Inhaled Pharmaceutical Aerosols, Academic Press, London, 2001, pp. 221-276.

[9] C. A. Dunber, A. J. Hickey, P. Holzner, Dispersion and Characterization of Pharmaceutical Dry Powder Aerosols, KONA Powder and Particle Journal, 16 (1998) 7-45.

[10] A. Gianfrancesco, C. Turchiuli, E. Dumoulin, Powder agglomeration during the spray-drying process: measurements of air properties, Dairy Science and Technology, 88 (2008) 53-64.

[11] Y. Ding, B. Stahlmecke, A. S. Jiménez, I. L. Tuinman, H. Kaminski, T. a. J. Kuhlbusch, M. Van Tongeren, M. Riediker, Dustiness and Deagglomeration Testing: Interlaboratory Comparison of Systems for Nanoparticle Powders, Aerosol Science and Technology, 49 (2015) 1222-1231.

[12] J. A. Quevedo, A. Omosebi, R. Pfeffer, Fluidization enhancement of agglomerates of metal oxide nanopowders by microjets, AIChE Journal, 56 (2010) 1456-1468.

[13] R. Hong, J. Ding, H. Li, Fluidization of fine powders in fluidized beds with an upward or a downward air jet, China Particuology, 3 (2005) 181-186.

[14] R. Pfeffer, J. A. Quevedo, J. Flesch, Fluidized bed systems and methods including micro-jet flow, U.S. patent No. US8118243B2, USA, 2008.

[15] J. Mcmillan, C. Briens, F. Berruti, E. Chan, High velocity attrition nozzles in fluidized beds, Powder Technology, 175 (2007) 133-141.

[16] L. Chen, H. Weinstein, Shape and extent of the void formed by a horizontal jet in a fluidized bed, AIChE Journal, 39 (1993) 1901-1909.

[17] H. Nasri Lari, J. Chaouki, J. R. Tavares, De-agglomeration of nanoparticles in a jet impactor-assisted fluidized bed, Powder Technology, 316 (2017) 455-461.

[18] J. R. V. Ommen, R. Pfeffer, Fluidization of nanopowders: experiments, modeling, and applications, 13th International Conference on Fluidized Bed Technology, December 2010.

[19] Z. Shen, C. L. Briens, M. Kwauk, M. A. Bergougnou, Study of a downward gas jet in a two-dimensional fluidized bed, The Canadian Journal of Chemical Engineering, 68 (1990) 534-540.

[20] Z. Shen, C. L. Briens, M. A. Bergougnou, M. Kwauk, Study of a downward grid jet in a large two-dimensional gas-fluidized bed, Powder Technology, 62 (1990) 227-234.

[21] J. A. Quevedo, R. Pfeffer, In Situ Measurements of Gas Fluidized Nanoagglomerates, Industrial & Engineering Chemistry Research, 49 (2010) 5263-5269.

[22] D. M. K. J. Ruud Van Ommen, Alan Weimer, Robert Pfeffer, Berend Van Wachem, Experiments and modelling of micro-jet assisted fluidization of nanoparticles, (2010).

[23] B. Esmaeili, J. Chaouki, C. Dubois, An evaluation of the solid hold-up distribution in a fluidized bed of nanoparticles using radioactive densitometry and fibre optics, The Canadian Journal of Chemical Engineering, 86 (2008) 543-552.

[24] M. Rasouli, O. Dubé, F. Bertrand, J. Chaouki, Investigating the dynamics of cylindrical particles in a rotating drum using multiple radioactive particle tracking, AIChE Journal, 62 (2016) 2622-2634.

[25] R. F. Mudde, W. K. Harteveld, H. E. A. Van Den Akker, T. H. J. J. Van Der Hagen, H. Van Dam, Gamma radiation densitometry for studying the dynamics of fluidized beds, Chemical Engineering Science, 54 (1999) 2047-2054.

[26] B. Koeninger, T. Hensler, S. Schug, W. Arlt, K.-E. Wirth, Horizontal secondary gas injection in fluidized beds: Solid concentration and velocity in multiphase jets, Powder Technology, 316 (2017) 49-58.

[27] A. Efhaima, M. H. Al-Dahhan, Local time-averaged gas holdup in fluidized bed reactor using gamma ray computed tomography technique (CT), International Journal of Industrial Chemistry, 6 (2015) 143-152.

[28] V. Jiradilok, D. Gidaspow, J. Kalra, S. Damronglerd, S. Nitivattananon, Explosive dissemination and flow of nanoparticles, Powder Technology, 164 (2006) 33-49.

[29] H. Nasri Lari, J. Chaouki, J. R. Tavares, Continuous aerosol photopolymerization to coat de-agglomerated nanoparticles, Chemical Engineering Journal, 390 (2020) 124526.

[30] G. F. Knoll, Radiation Detection and Measurement, Wiley, Hoboken, N.J., 2010.

[31] W. C. Yang, Handbook of Fluidization and Fluid-Particle Systems, Taylor & Francis 2003.

[32] D. a. a. D. Vasconcelos, M. M. Hamada, C. H. Mesquita, C. C. Dantas, R. Narain, S. B. Melo, V. a. D. Santos, Collimator design for single beam gamma ray industrial tomography and fan beam geometry, International Nuclear Atlantic Conference - INAC 2011Belo Horizonte, MG, Brazil, 2011.

[33] C. C. Xu, J. Zhu, Prediction of the Minimum Fluidization Velocity for Fine Particles of Various Degrees of Cohesiveness, Chemical Engineering Communications, 196 (2008) 499-517.

[34] W. Yao, G. Guangsheng, W. Fei, W. Jun, Fluidization and agglomerate structure of SiO_2 nanoparticles, Powder Technology, 124 (2002) 152-159.

[35] C. Zhu, Q. Yu, R. N. Dave, R. Pfeffer, Gas fluidization characteristics of nanoparticle agglomerates, AIChE Journal, 51 (2005) 426-439.

[36] I. Hirsan, C. Sishtla, T. M. Knowlton, Effect of bed and jet parameters on vertical jet penetration length in gas fluidized beds, 73. annual meeting of the American Institute of Chemical EngineersChicago, IL, USA, 1980.

[37] T. M. Knowlton, I. Hirsan, The Effect of Pressure on Jet Penetration in Semi-Cylindrical Gas-Fluidized Beds, (1980) 315-324.

[38] C. H. Wang, Z. P. Zhong, R. Li, J. Q. E, Prediction of jet penetration depth based on least square support vector machine, Powder Technology, 203 (2010) 404-411.

[39] C. S. Chyang, C. H. Chang, J. H. Chang, Gas discharge modes at a single horizontal nozzle in a two-dimensional fluidized bed, Powder Technology, 90 (1997) 71-77.

[40] B. Ettehadieh, D. Gidaspow, R. W. Lyczkowski, Hydrodynamics of fluidization in a semicircular bed with a jet, AIChE Journal, 30 (1984) 529-536.

[41] A. Efhaima, M. H. Al-Dahhan, Bed diameter effect on the hydrodynamics of gas-solid fluidized beds via radioactive particle tracking (RPT) technique, The Canadian Journal of Chemical Engineering, 95 (2017) 744-756.
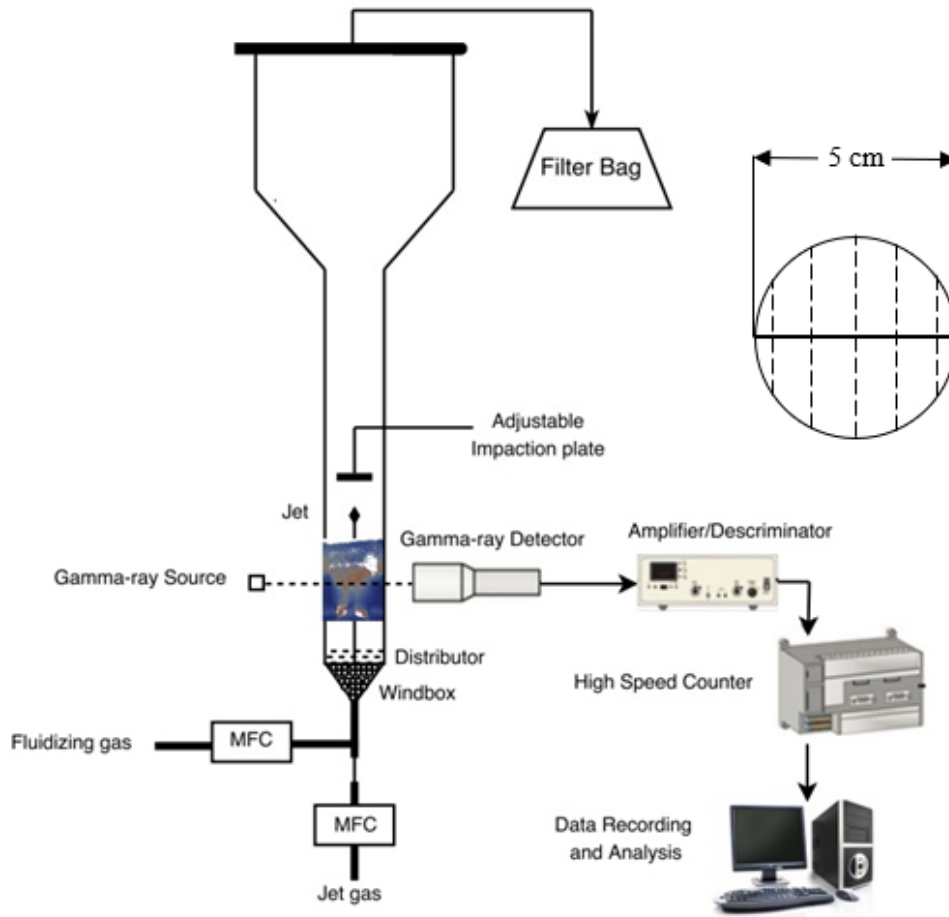
Figure 1

136x128mm (96 x 96 DPI)
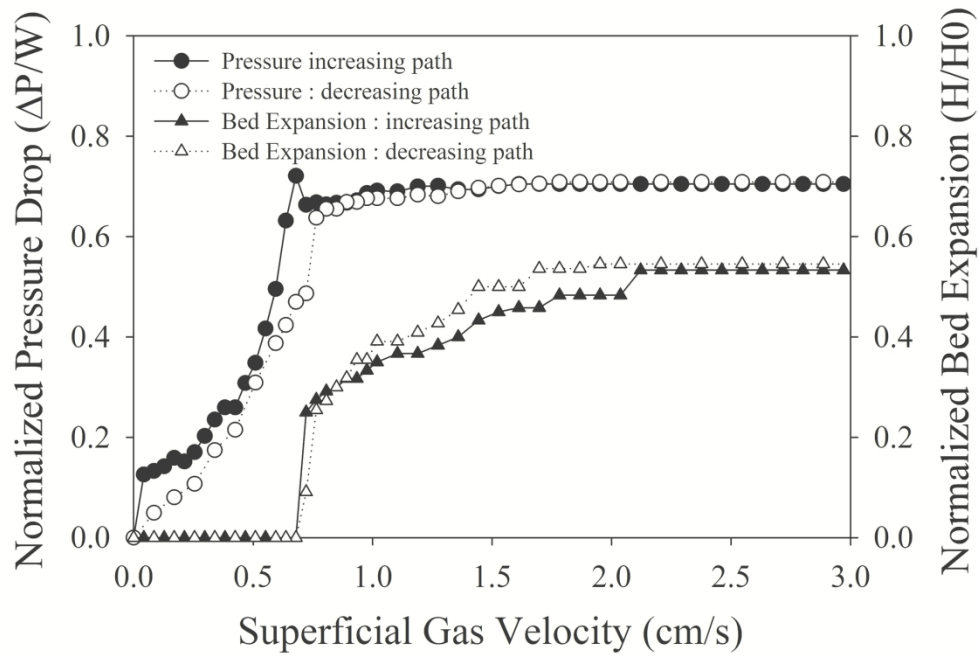
Figure 2a

177x121mm (300 x 300 DPI)
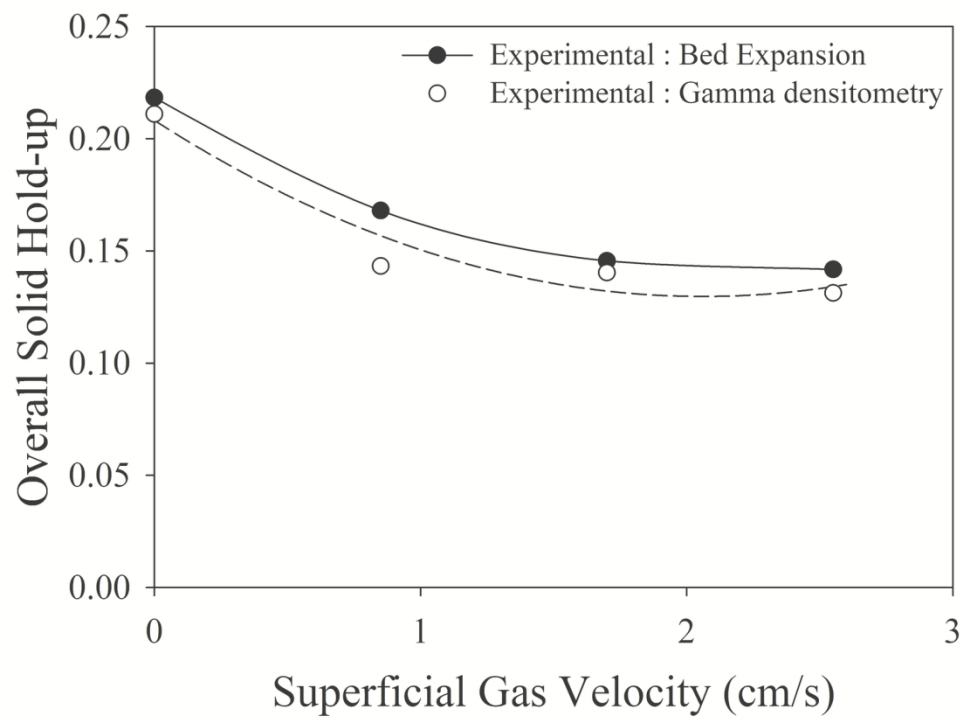
Figure 2b

158x115mm (300 x 300 DPI)

1
2
3
4
5
6
7
8
9
10
11
12
13
14
15
16
17
18
19
20
21
22
23
24
25
26
27
28
29
30
31
32
33
34
35
36
37
38
39
40
41
42
43
44
45
46
47
48
49
50
51
52
53
54
55
56
57
58
59
60
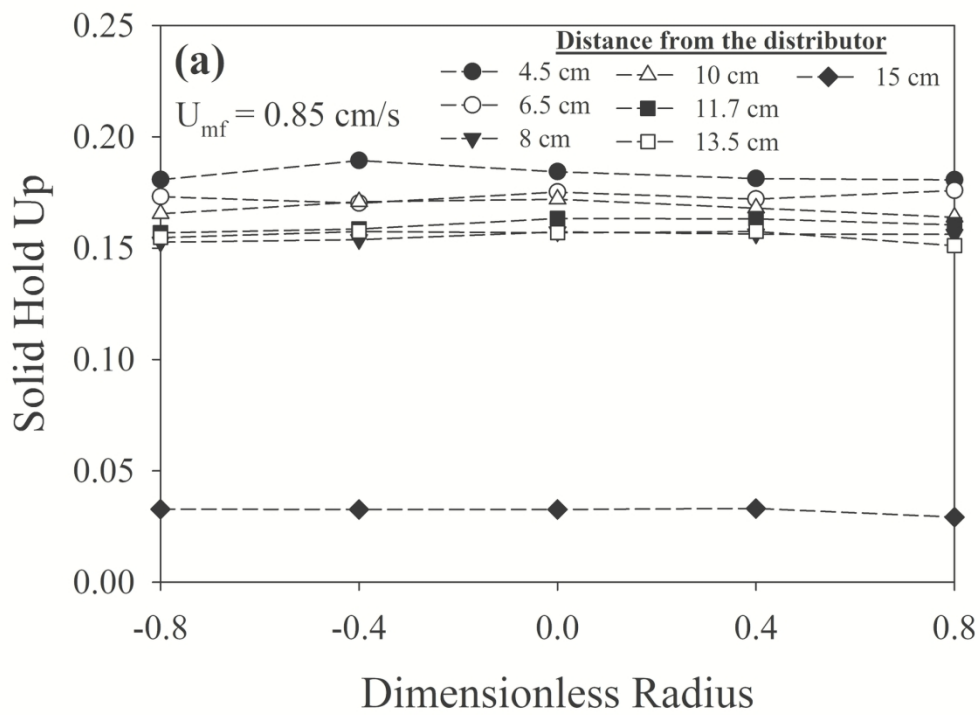
Figure 3a

159x119mm (300 x 300 DPI)
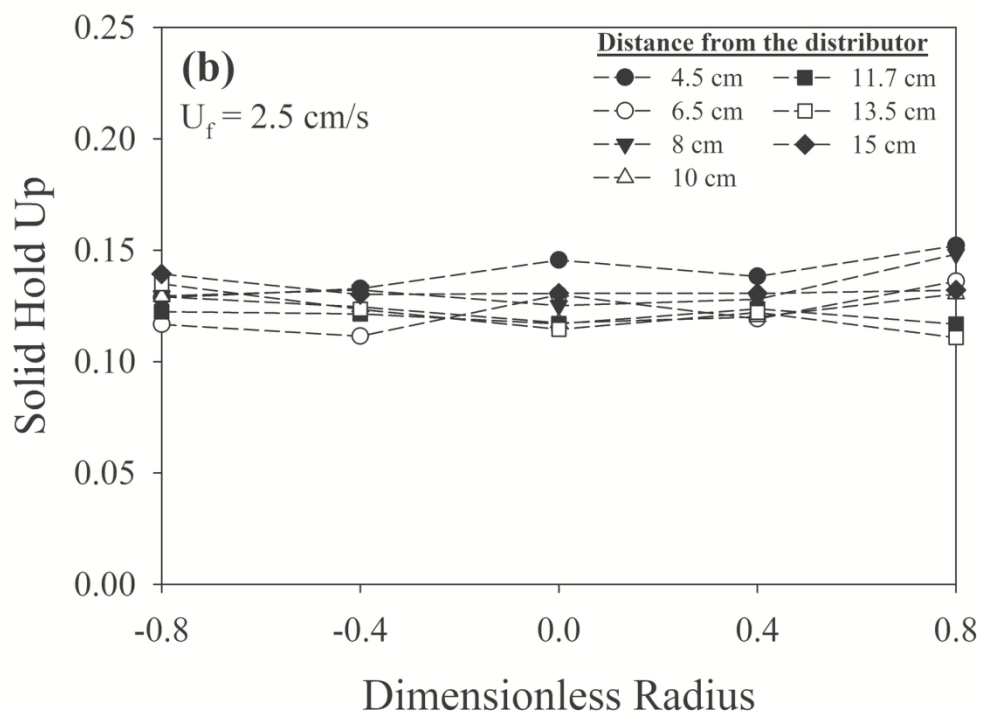
Figure 3b

159x121mm (300 x 300 DPI)
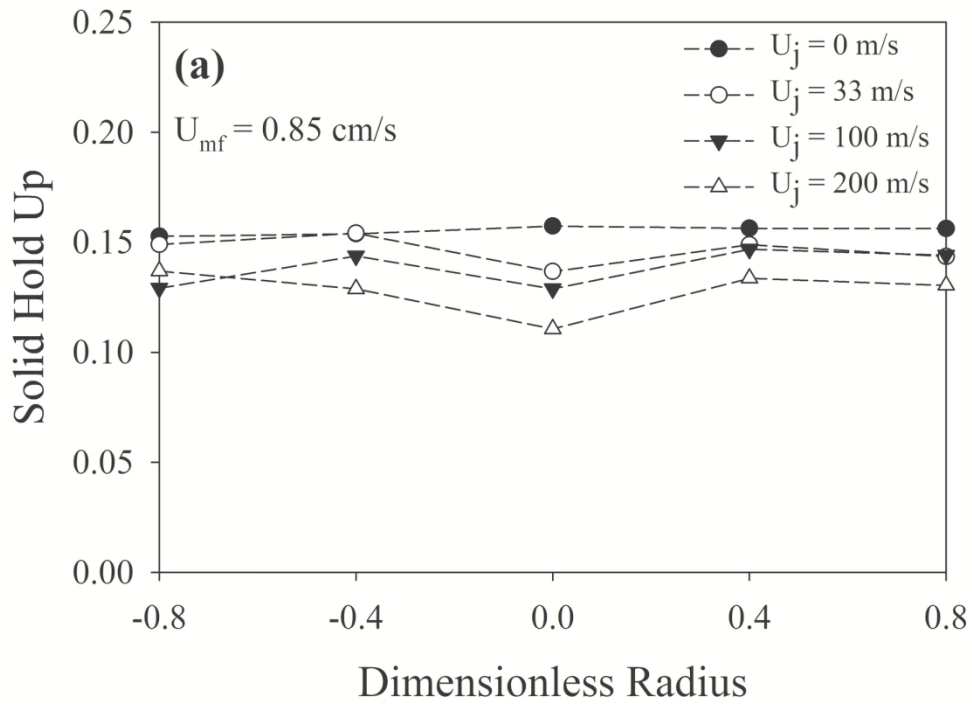
Figure 4a

161x117mm (300 x 300 DPI)
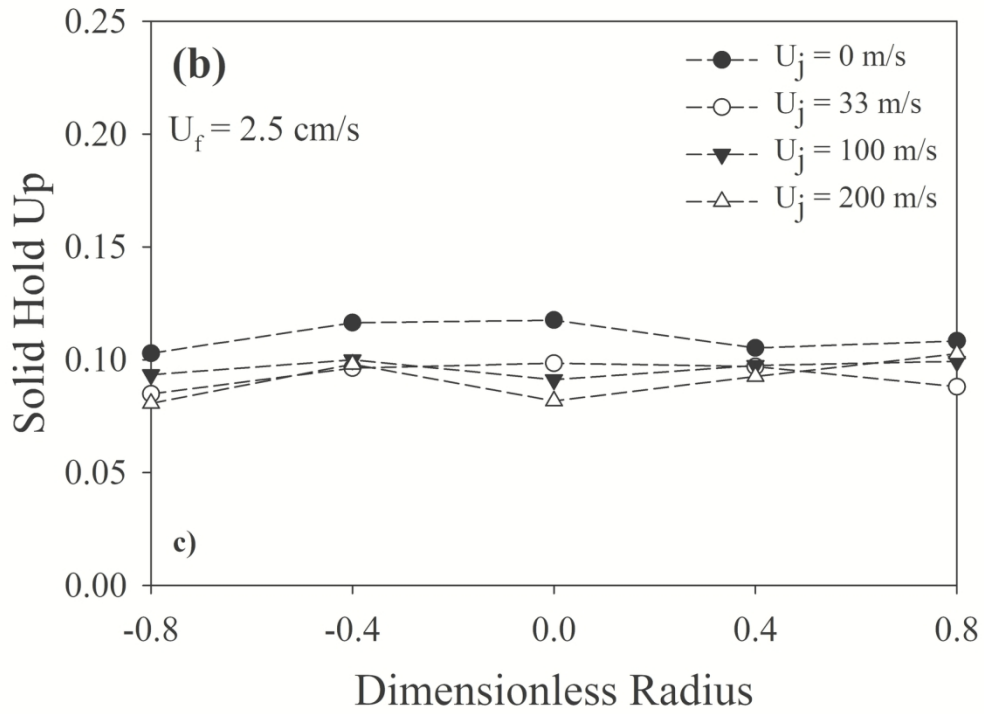
Figure 4b

157x118mm (300 x 300 DPI)
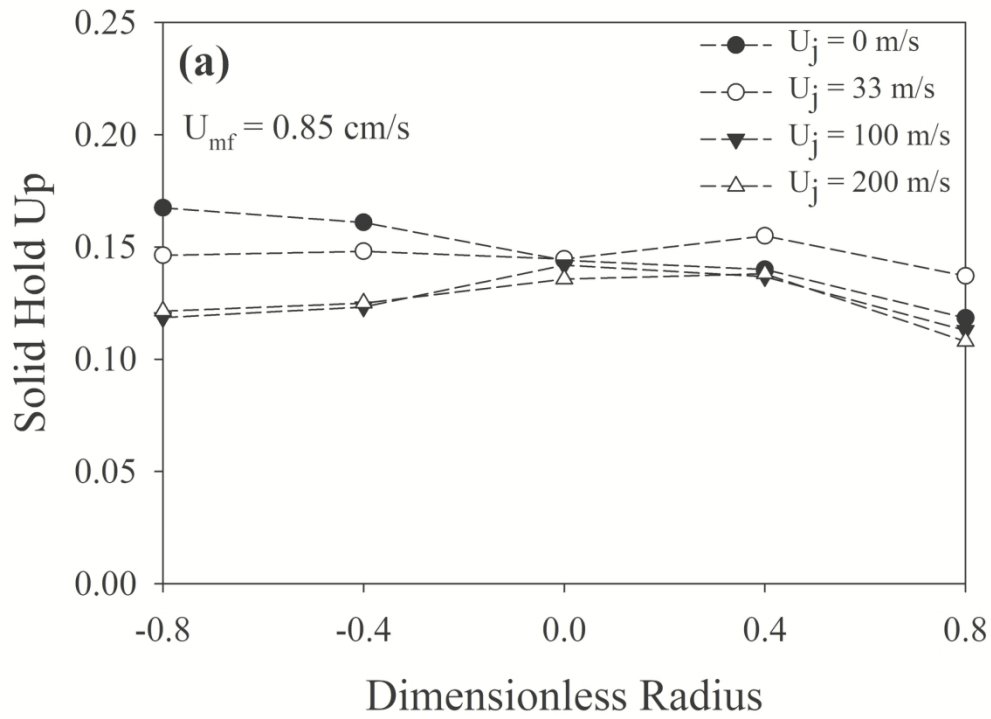
Figure 5a

158x119mm (300 x 300 DPI)
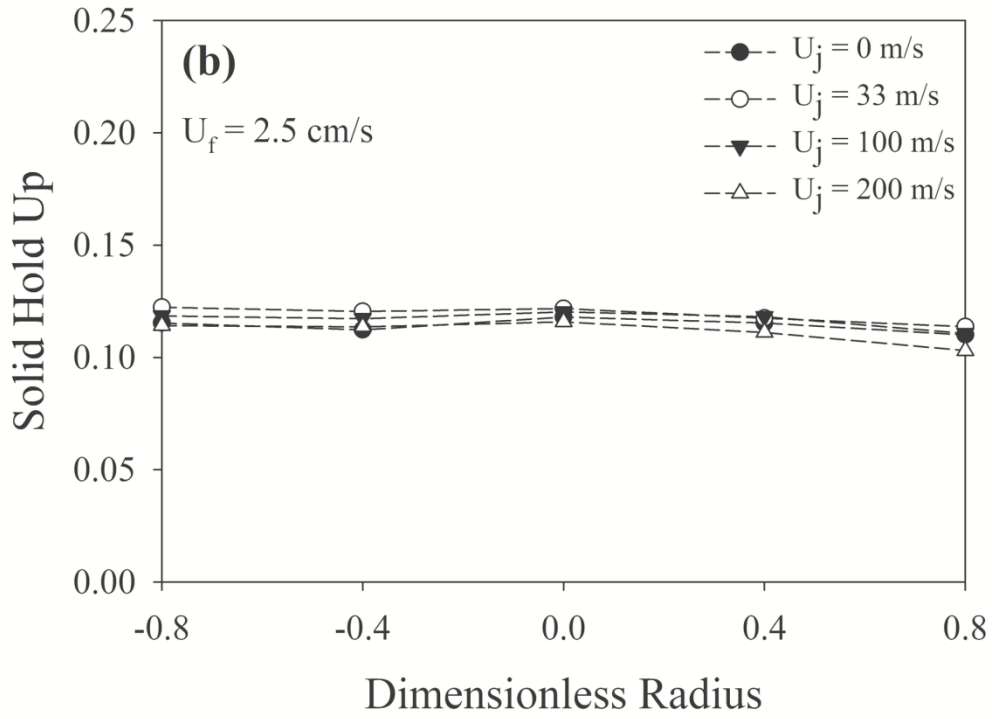
Figure 5b

157x118mm (300 x 300 DPI)

Figure 5c

57x56mm (96 x 96 DPI)
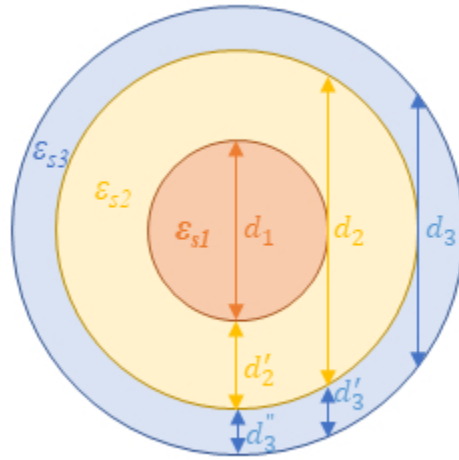
Figure 6a
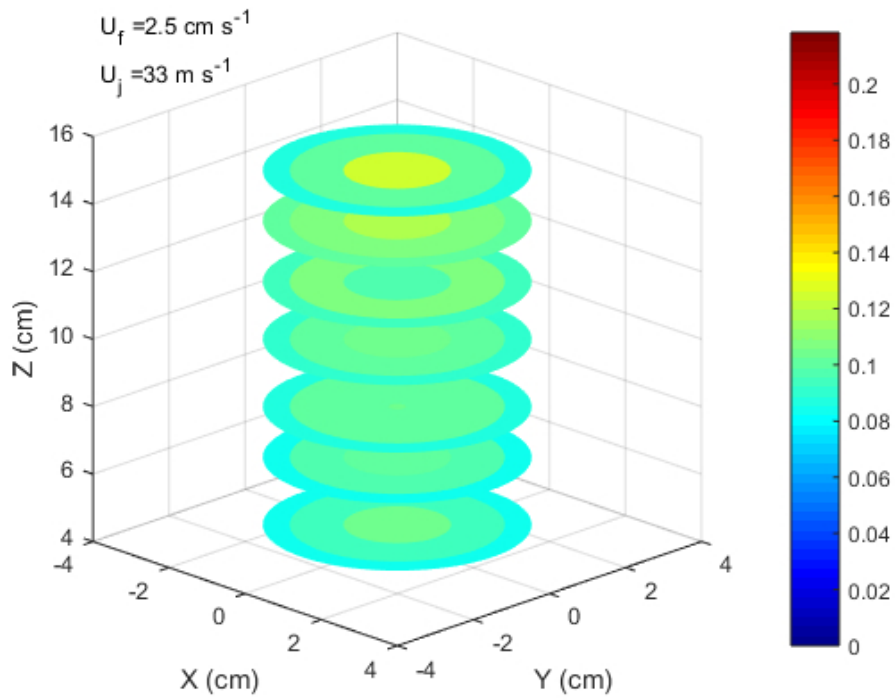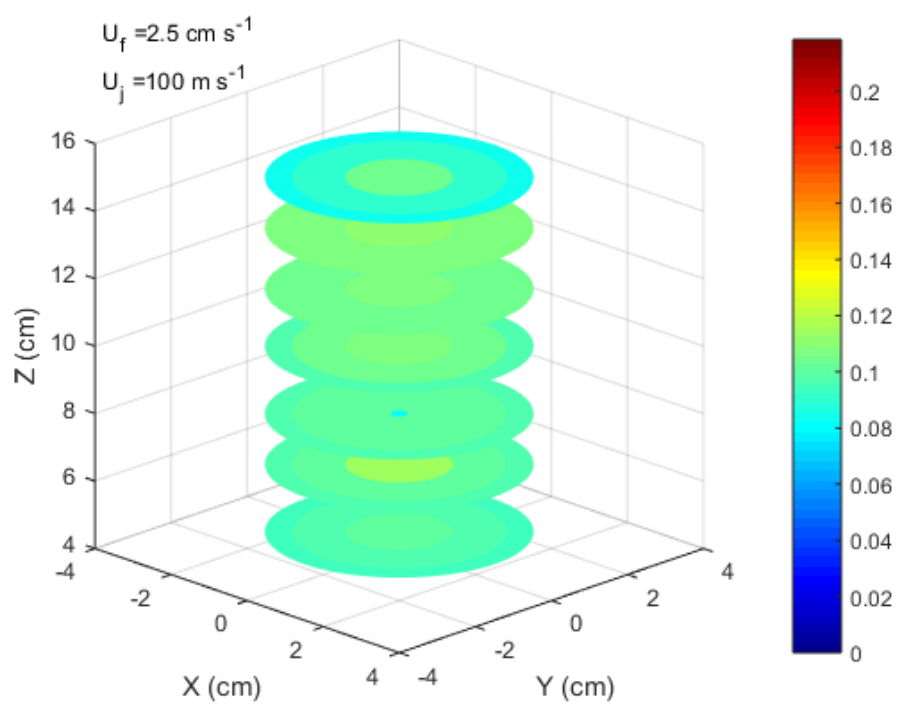
73x71mm (96 x 96 DPI)
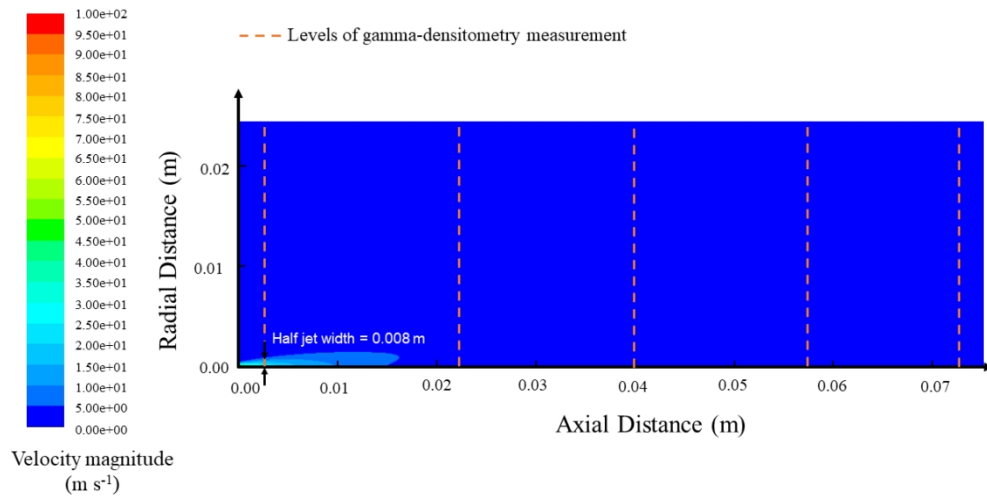
Figure 6b

338x190mm (96 x 96 DPI)
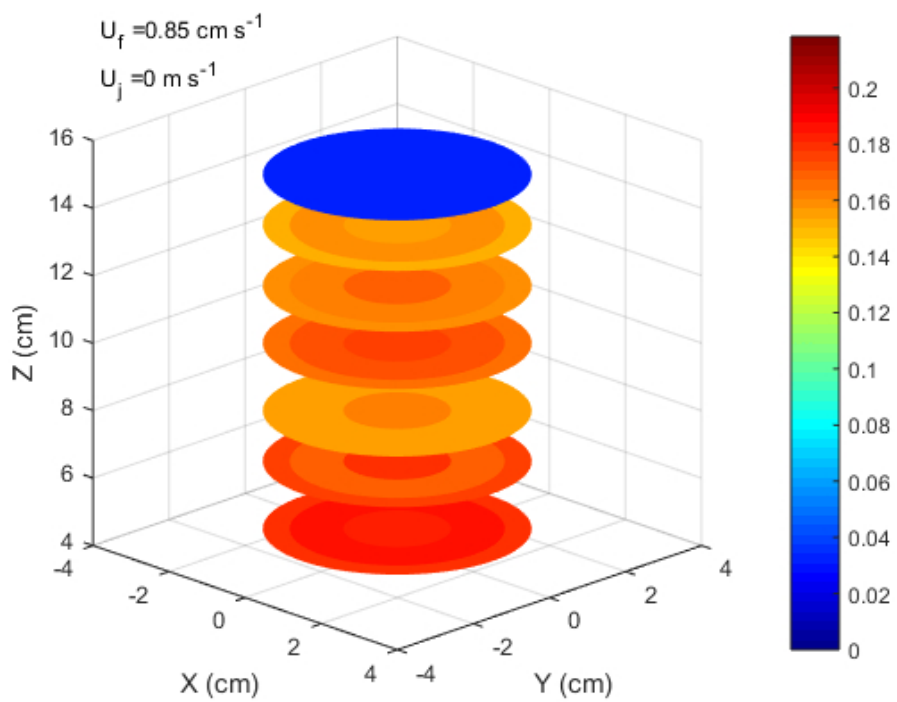
Figure 7a

148x111mm (96 x 96 DPI)
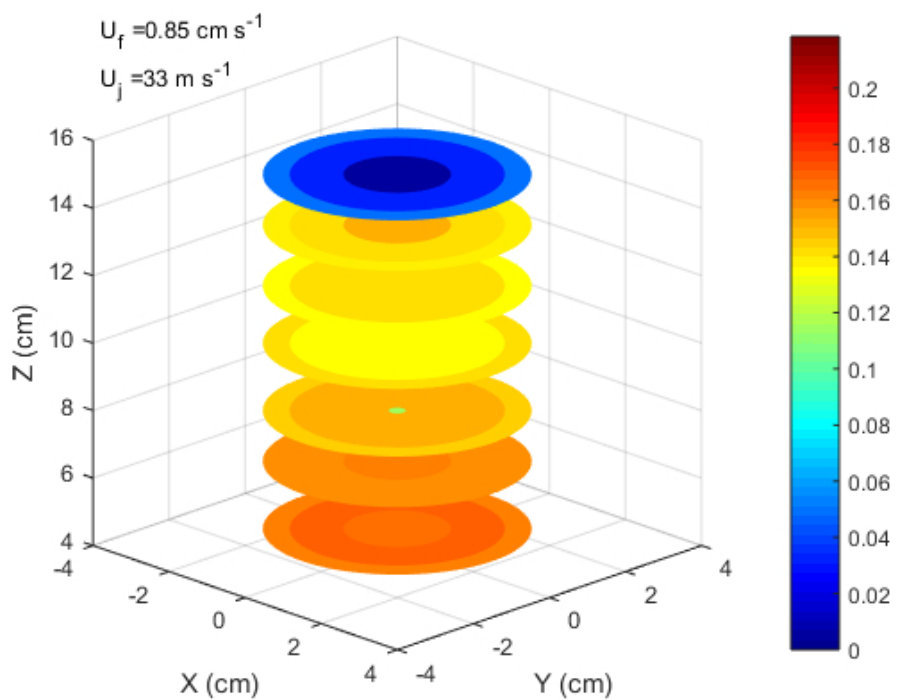
Figure 7b

148x111mm (96 x 96 DPI)

1
2
3
4
5
6
7
8
9
10
11
12
13
14
15
16
17
18
19
20
21
22
23
24
25
26
27
28
29
30
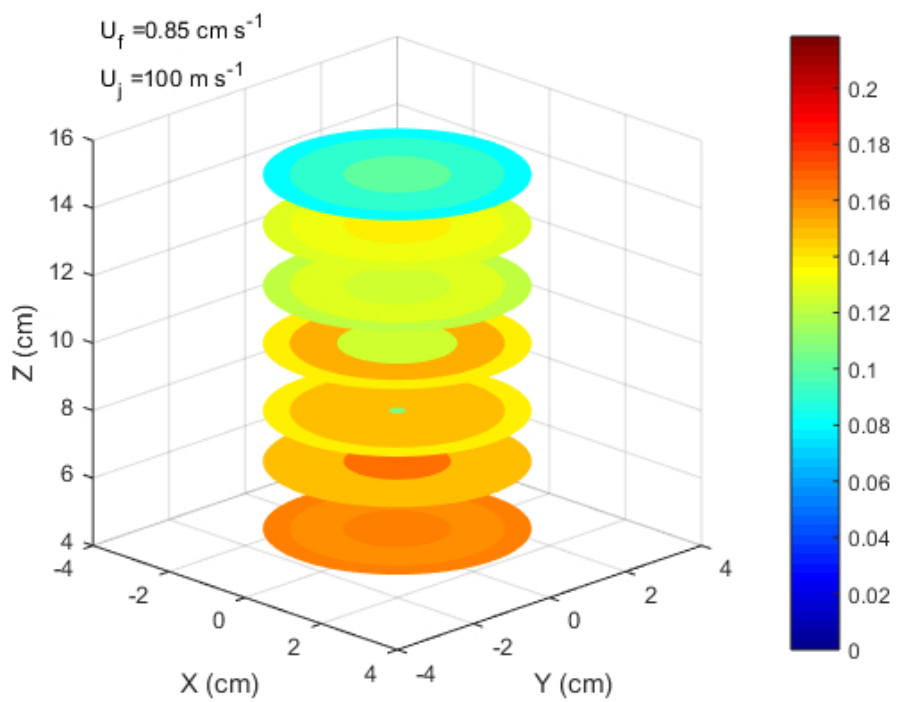
Figure 7c

148x111mm (96 x 96 DPI)

31
32
33
34
35
36
37
38
39
40
41
42
43
44
45
46
47
48
49
50
51
52
53
54
55
56
57
58
59
60
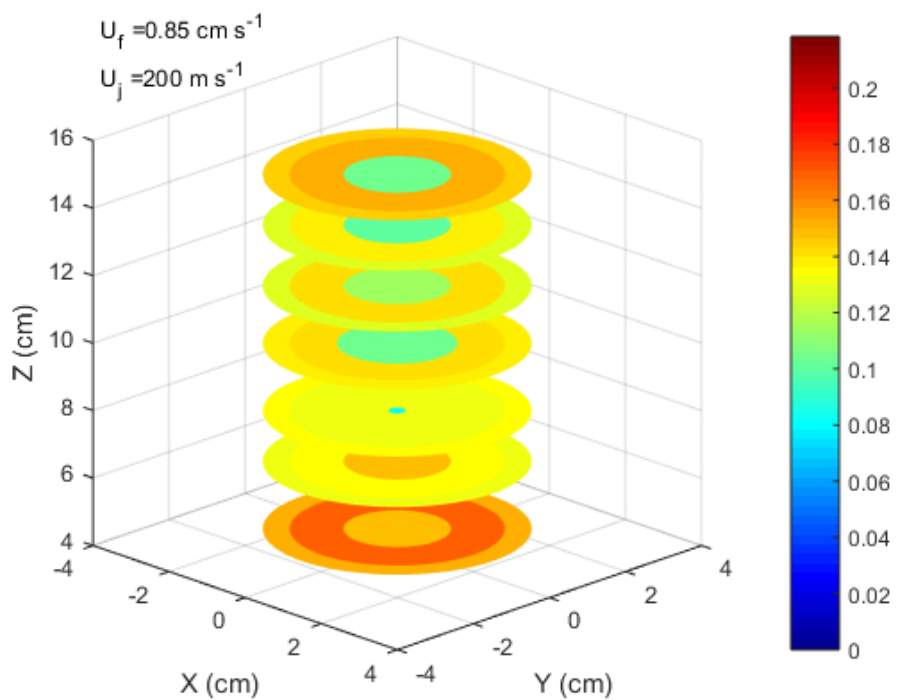
Figure 7d

148x111mm (96 x 96 DPI)
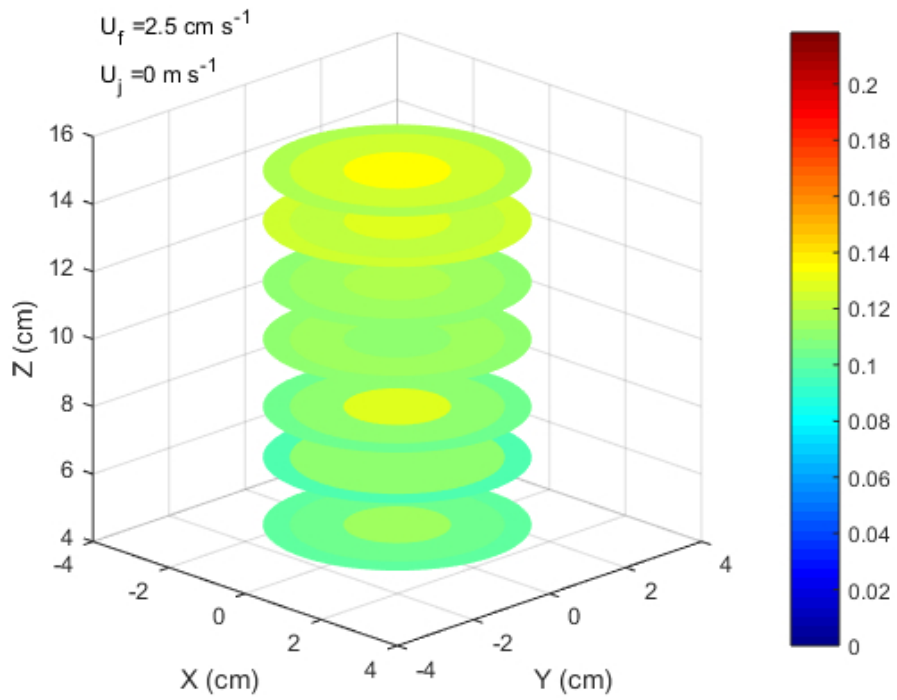
Figure 8a

148x111mm (96 x 96 DPI)

1
2
3
4
5
6
7
8
9
10
11
12
13
14
15
16
17
18
19
20
21
22
23
24
25
26
27
28
29
30
31
32
33
34
35
36
37
38
39
40
41
42
43
44
45
46
47
48
49
50
51
52
53
54
55
56
57
58
59
60

Figure 8b

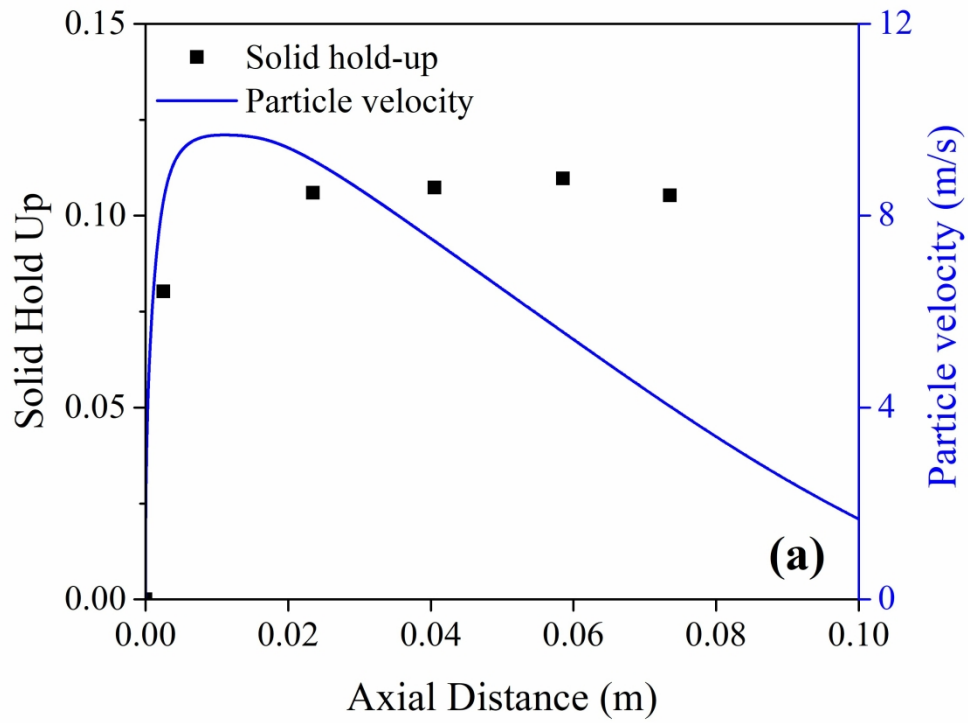148x111mm (96 x 96 DPI)

Figure 8c

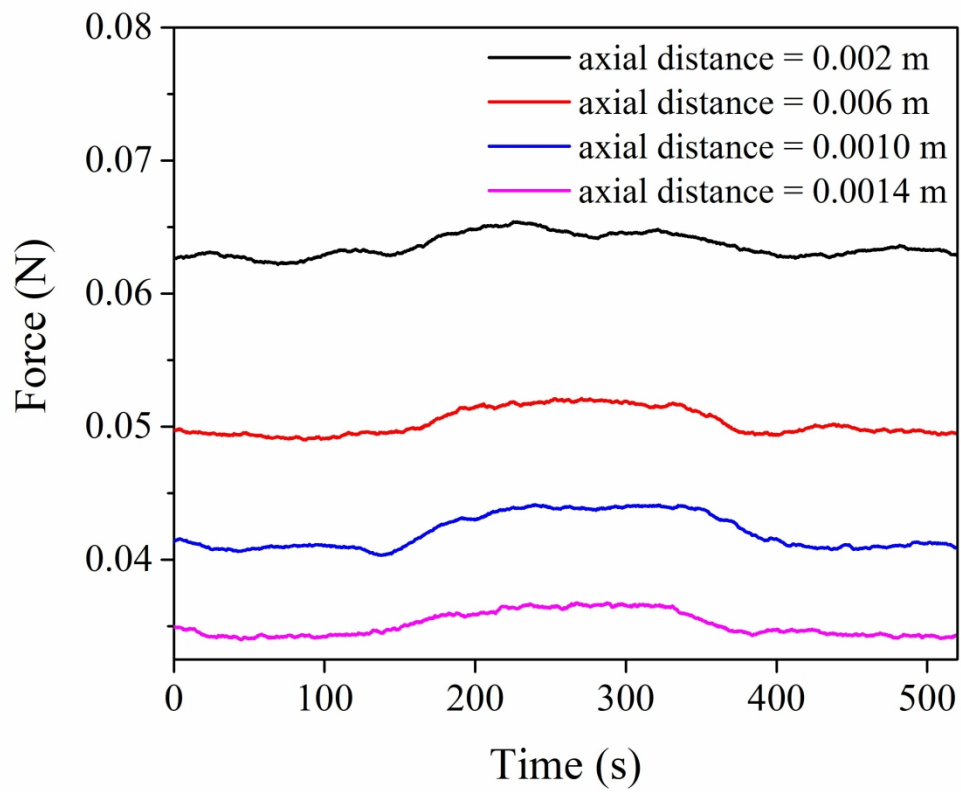148x111mm (96 x 96 DPI)
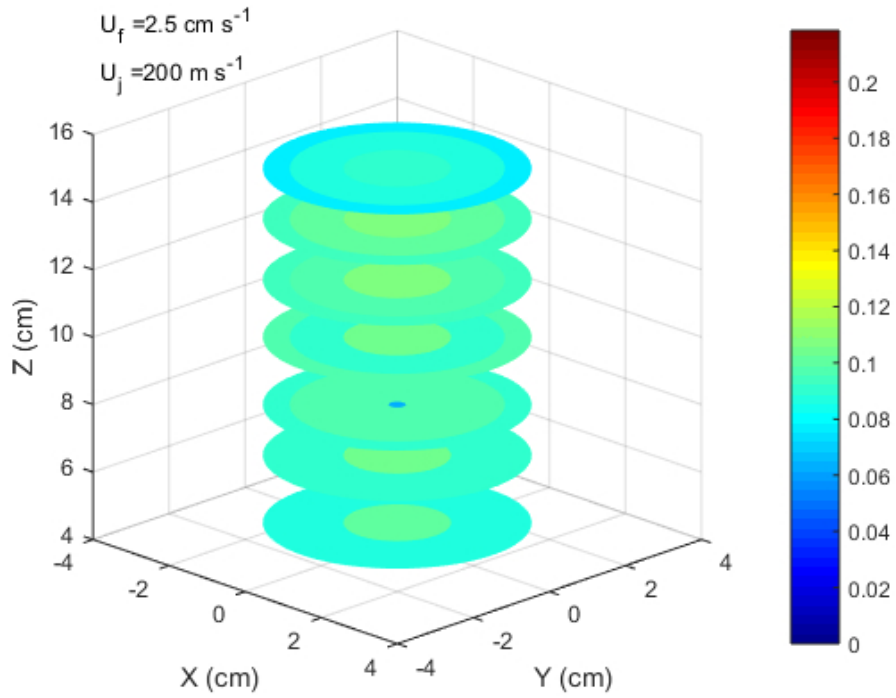
Figure 8d

148x111mm (96 x 96 DPI)

Figure 9a

Figure 9b

Figure 10